Electronic Supplementary Information section

Synthesis, structural characterization DFT analysis and study of binding interactions of new bicapped Keggin phosphotetradecavanadates

Rim Zarroug, Beñat Artetxe, Brahim Ayed, Xavier López, Nádia Ribeiro, Isabel Correia, João Costa Pessoa

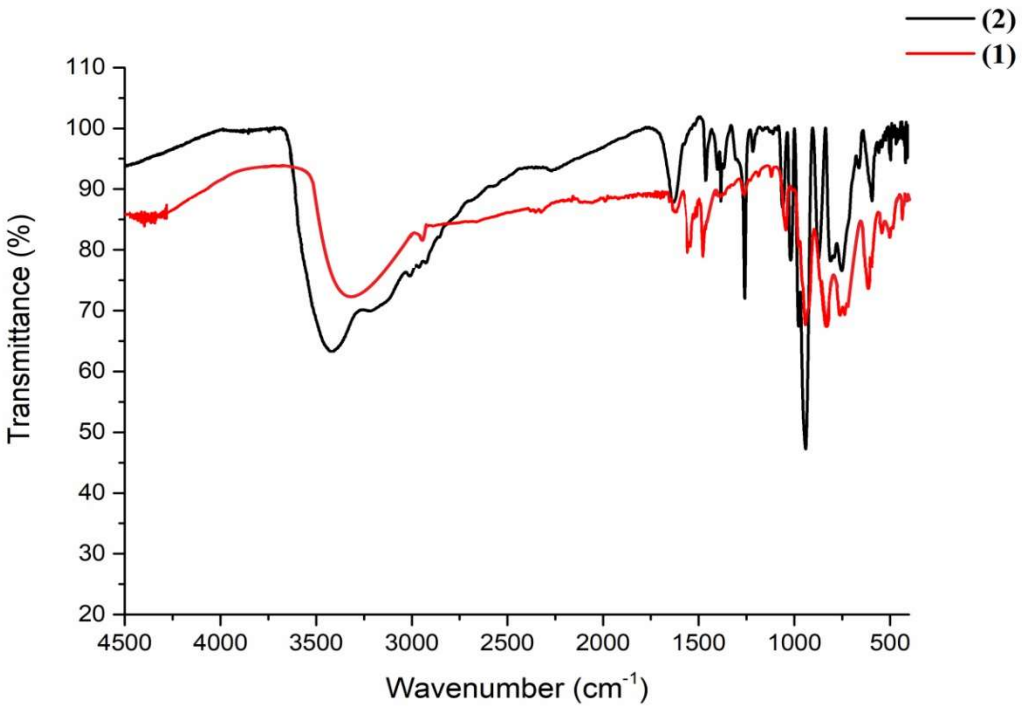

Fig. S1. FTIR spectra of compounds **1** and **2** measured in KBr disks.

Single crystal X-ray diffraction data

Table S1 Crystal data and structure refinement for compounds **1** and **2**.

	Compound 1	**Compound 2**
Empirical formula	$(C_6H_8N)_5[H_4PV_{14}O_{42}]\cdot 5H_2O$	$(C_6H_{14}N_4)_2(NH_4)[H_4PV_{14}O_{42}]\cdot 11H_2O$
Formula weight ($g.mol^{-1}$)	1980.91	1920.8
Temperature (K)	100	100
Crystal system	Monoclinic	Triclinic
Space group	$P2_1/c$	P-1
a (Å)	14.0745(3)	11.1991 (8)
b (Å)	34.2555(5)	11.4892 (9)
c (Å)	14.1623(3)	13.4138 (14)
α (°)	90	67.429 (8)
β (°)	115.364(2)	66.782 (8)
γ (°)	90	85.757 (6)
V ($Å^3$)	6169.9(2)	1458.6 (2)
ρ_{calcd} ($g\ cm^{-3}$)	2.133	2.229
Z	4	1
μ (mm^{-1})	2.153	2.287
F(000)	3928	954
Index ranges	$-17 \le h \le 17$; $-40 \le k \le 41$; $-16 \le l \le 17$	$-13 \le h \le 13$; $-11 \le k \le 14$; $-16 \le l \le 16$
Reflections collected	45032	10022
Unique reflections (R_{int})	11472 (0.081)	5613 (0.054)
Observed reflections $[I > 2\sigma(I)]$	9024	3550
Parameters (restraints)	914 (50)	478 (62)
$R(F)$[a] $[I > 2\sigma(I)]$	0.056	0.077
$wR(F^2)$[b] [all data]	0.143	0.233
Goodness of Fit	1.071	1.030
$\Delta\rho_{max}/\Delta\rho_{min}$ ($eÅ^{-3}$)	2.30 /-0.84	2.11/-1.13

(a) $R(F)=\Sigma||F_o|-|F_c||/\Sigma|F_o|$; **(b)** $wR(F^2)=\{\Sigma[w(F_o^2-F_c^2)^2]/\Sigma[w(F_o^2)^2]\}^{1/2}$

Table S2 Selected bond lengths [Å] for the anion in compound **1** (Å)

Bond length (Å)	***X-ray***	***Bond length (Å)***	***X-ray***
V1—O23	1.602 (4)	V8—O4	1.833 (4)
V1—O22	1.728 (4)	V8—O1	1.874 (4)
V1—O25	1.916 (4)	V8—O2	1.915 (4)
V1—O2	1.943 (4)	V9—O35	1.616 (4)
V1—O4	2.070 (4)	V9—O27	1.721 (4)
V1—O7	2.371 (4)	V9—O15	1.920 (4)
V2—O21	1.616 (4)	V9—O20	1.933 (4)
V2—O25	1.727 (4)	V9—O13	2.024 (4
V2—O6	1.880 (3)	V9—O9	2.323 (4)
V2—O19	1.966 (4)	V10—O39	1.597 (4)
V2—O8	2.03 (4)	V10—O28	1.740 (4)
V2—O3	2.360 (4)	V10—O27	1.927 (4)
V3—O14	1.600 (4)	V10—O5	1.932 (4)
V3—O6	1.731 (4)	V10—O16	2.045 (4)
V3—O4	1.914 (4)	V10—O11	2.386 (4)
V3—O1	1.967 (4)	V11—O37	1.594 (4)
V3—O9	2.061 (4)	V11—O20	1.746 (4)
V4—O30	1.601 (4)	V11—O33	1.914 (4)
V4—O19	1.747 (4)	V11—O1	1.922 (4)
V4—O12	1.892 (4)	V11—O18	2.047 (4)
V4—O17	1.955 (4)	V11—O9	2.408 (3)
V4—O10	2.050 (4)	V12—O34	1.594 (4)
V4—O3	2.380 (3)	V12—O38	1.724 (4)
V5—O31	1.602 (4)	V12—O29	1.928 (4)
V5—O15	1.731 (4)	V12—O18	1.958 (4)
V5—O8	1.927 (4)	V12—O2	2.065 (4)
V5—O16	1.945 (4)	V12—O7	2.354 (4)
V5—O17	2.065 (4)	V13—O42	1.617 (4)
V5—O3	2.352 (4)	V13—O10	1.822 (4)
V6—O32	1.596 (4)	V13—O16	1.836 (4)

V6—O12	1.764 (4)	V13—O5	1.871 (4)
V6—O26	1.905 (4)	V13—O17	1.949 (4)
V6—O22	1.937 (4)	V14—O41	1.615 (4)
V6—O29	1.975 (4)	V14—O33	1.702 (4)
V6—O7	2.430 (3)	V14—O38	1.916 (4)
V7—O36	1.598 (4)	V14—O28	1.935 (4)
V7—O26	1.721 (4)	V14—O24	2.369 (4)
V7—O24	1.923 (4)	V14—O11	2.369 (4)
V7—O10	1.968 (4)	P—O7	1.532 (4)
V7—O5	2.075 (4)	P—O11	1.534 (4)
V7—O11	2.377 (4)	P—O9	1.539 (4)
V8—O40	1.614 (4)	P—O3	1.543 (4)
V8—O18	1.815 (4)		

Table S3 Selected bond angles [°] for compound **1**.

Bond angles [°]		Bond angles [°]	
O23—V1—O22	101.51 (18)	O40—V8—O18	115.25 (19)
O23—V1—O25	101.52 (18)	O40—V8—O4	116.51 (18)
O22—V1—O25	94.04 (17)	O18—V8—O4	128.17 (17)
O23—V1—O2	101.13 (17)	O40—V8—O1	104.69 (18)
O22—V1—O2	99.86 (17)	O18—V8—O1	84.88 (17)
O25—V1—O2	150.39 (16)	O4—V8—O1	84.81 (16)
O23—V1—O4	96.46 (16)	O40—V8—O2	102.72 (18)
O22—V1—O4	162.03 (16)	O18—V8—O2	83.68 (16)
O25—V1—O4	82.41 (15)	O4—V8—O2	82.87 (16)
O2—V1—O4	76.31 (15)	O1—V8—O2	152.59 (16)
O23—V1—O7	172.99 (17)	O35—V9—O27	103.88 (19)
O22—V1—O7	78.10 (15)	O35—V9—O15	101.07 (19)
O25—V1—O7	85.49 (14)	O27—V9—O15	90.27 (17)
O2—V1—O7	72.15 (14)	O35—V9—O20	95.50 (19)
O4—V1—O7	84.05 (13)	O27—V9—O20	97.32 (18)
O21—V2—O25	103.81 (18)	O15—V9—O20	159.57 (16)
O21—V2—O6	101.77 (18)	O35—V9—O13	95.12 (18
O25—V2—O6	92.12 (16)	O27—V9—O13	160.93 (17)

O21—V2—O19	96.45 (17)	O15—V9—O13	84.44 (16)
O25—V2—O19	93.93 (16)	O20—V9—O13	82.24 (16)
O6—V2—O19	158.83 (16)	O35—V9—O9	164.86 (17)
O21—V2—O8	94.99 (17)	O27—V9—O9	89.87 (16)
O25—V2—O8	161.09 (17)	O15—V9—O9	84.92 (14)
O6—V2—O8	85.94 (15)	O20—V9—O9	76.19 (14)
O19—V2—O8	81.79 (15)	O13—V9—O9	71.44 (14)
O21—V2—O3	164.59 (16)	O39—V10—O28	101.7 (2)
O25—V2—O3	89.25 (15)	O39—V10—O27	102.69 (19)
O6—V2—O3	85.62 (14)	O28—V10—O27	92.73 (18)
O19—V2—O3	74.20 (14)	O39—V10—O5	100.29 (18)
O8—V2—O3	71.85 (14)	O28—V10—O5	99.46 (18)
O14—V3—O6	104.40 (19)	O27—V10—O5	151.17 (16)
O14—V3—O13	97.50 (19)	O39—V10—O16	96.84 (19)
O6—V3—O13	96.06 (17)	O28—V10—O16	161.47 (17)
O14—V3—O4	101.07 (18)	O27—V10—O16	82.02 (16)
O6—V3—O4	91.49 (16)	O5—V10—O16	78.15 (16)
O13—V3—O4	157.53 (17)	O39—V10—O11	173.09 (17)
O14—V3—O1	97.90 (17)	O28—V10—O11	78.25 (15)
O6—V3—O1	156.44 (16)	O27—V10—O11	84.20 (14)
O13—V3—O1	88.38 (16)	O5—V10—O11	73.00 (14)
O4—V3—O1	76.68 (14)	O16—V10—O11	83.53 (14)
O14—V3—O9	164.00 (16)	O37—V11—O20	100.9 (2)
O6—V3—O9	88.79 (15)	O37—V11—O33	102.95 (19)
O13—V3—O9	71.71 (15)	O20—V11—O33	92.62 (18)
O4—V3—O9	87.37 (14)	O37—V11—O1	101.36 (18)
O1—V3—O9	70.61 (13)	O20—V11—O1	99.17 (17)
O30—V4—O19	101.13 (19	O33—V11—O1	150.35 (16)
O30—V4—O12	102.03 (18)	O37—V11—O18	98.05 (19)
O19—V4—O12	95.76 (17)	O20—V11—O18	160.99 (16)
O30—V4—O17	98.85 (18)	O33—V11—O18	82.41 (16)
O19—V4—O17	97.65 (17)	O1—V11—O18	77.62 (15)
O12—V4—O17	152.45 (16)	O37—V11—O9	172.89 (18)

O30—V4—O10	96.71 (18)	O20—V11—O9	77.25 (15)
O19—V4—O10	162.06 (16)	O33—V11—O9	84.04 (14)
O12—V4—O10	82.30 (16)	O1—V11—O9	72.34 (13)
O17—V4—O10	77.56 (15)	O18—V11—O9	83.97 (13)
O30—V4—O3	170.32 (18)	O34—V12—O38	104.4 (2)
O19—V4—O3	77.44 (14)	O34—V12—O29	96.98 (19)
O12—V4—O3	87.65 (14)	O38—V12—O29	97.92 (18)
O17—V4—O3	72.03 (13)	O34—V12—O18	100.18 (19)
O10—V4—O3	84.65 (13)	O38—V12—O18	90.85 (17)
O31—V5—O15	104.53 (19)	O29—V12—O18	158.14 (16)
O31—V5—O8	97.53 (18)	O34—V12—O2	96.73 (18)
O1—V5—O8	96.33 (16)	O38—V12—O2	157.03 (18)
O1—V5—O16	98.99 (19)	O29—V12—O2	88.26 (16)
O6—V5—O16	91.92 (17)	O18—V12—O2	76.41 (15)
O6—V5—O16	159.05 (16)	O34—V12—O7	164.04 (18)
O31—V5—O17	96.13 (17)	O38—V12—O7	89.87 (16)
O15—V5—O17	157.77 (17)	O29—V12—O7	73.59 (14)
O8—V5—O17	88.92 (15)	O18—V12—O7	86.51 (14)
O16—V5—O17	76.60 (15)	O2—V12—O7	70.59 (13)
O31—V5—O3	164.16 (16)	O42—V13—O10	115.33 (19)
O15—V5—O3	89.81 (15)	O42—V13—O16	117.18 (19)
O8—V5—O3	73.80 (14)	O10—V13—O16	127.18 (17)
O16—V5—O3	87.04 (14)	O42—V13—O5	106.0 (2)
O32—V6—O12	103.32 (19)	O10—V13—O5	86.00 (17)
O32—V6—O26	100.96 (19)	O16—V13—O5	85.16 (17)
O12—V6—O26	90.87 (17)	O42—V13—O17	100.5 (2)
O32—V6—O22	99.17 (18)	O10—V13—O17	83.38 (16)
O12—V6—O22	93.22 (17)	O16—V13—O17	82.09 (16)
O26—V6—O22	157.93 (16)	O5—V13—O17	153.48 (16)
O32—V6—O29	96.94 (19)	O41—V14—O33	104.0 (2)
O12—V6—O29	159.70 (16)	O41—V14—O38	100.7 (2)
O26—V6—O29	86.33 (17)	O33—V14—O38	91.95 (18)
O22—V6—O29	82.34 (16)	O41—V14—O28	97.4 (2)

O32—V6—O7	166.23 (17)	O33—V14—O28	97.05 (18)
O12—V6—O7	88.68 (14)	O38—V14—O28	157.24 (17)
O26—V6—O7	85.36 (14)	O41—V14—O24	94.9 (2)
O22—V6—O7	73.07 (13)	O33—V14—O24	161.02 (18)
O29—V6—O7	71.07 (14)	O38—V14—O24	82.64 (17)
O36—V7—O26	104.73 (19)	O28—V14—O24	82.11 (17)
O36—V7—O24	98.2 (2)	O41—V14—O11	164.83 (18)
O26—V7—O24	97.67 (19)	O33—V14—O11	90.22 (16)
O36—V7—O10	100.00 (19)	O38—V14—O11	83.83 (15)
O26—V7—O10	90.24 (17)	O28—V14—O11	75.30 (14)
O24—V7—O10	157.56 (17)	O24—V14—O11	71.16 (15)
O36—V7—O5	94.86 (18)	O7—P—O11	108.7 (2)
O26—V7—O5	158.29 (17)	O7—P—O9	110.3 (2)
O24—V7—O5	88.53 (18)	O11—P—O9	109.67 (19)
O10—V7—O5	77.03 (15)	O7—P—O3	109.3 (2)
O36—V7—O11	163.07 (18)	O11—P—O3	110.7 (2)
O26—V7—O11	90.96 (15)	O9—P—O3	108.1 (2)
O24—V7—O11	72.93 (16)		
O10—V7—O11	86.03 (14)		
O5—V7—O11	70.92 (13)		

Table S4 Selected bond lengths [Å] for the anion in compound **2** (Å)

	Bond length (Å)		**Bond length (Å)**
V1—O15	1.585 (7)	V5—O2	1.592 (6)
V1—O6	1.770 (7)	V5—O18	1.825 (8)
V1—O11	1.820 (8)	V5—O14	1.851 (7)
V1—O4	1.989 (7)	V5—O23^{i}	2.416 (12)
V1—O9	2.027 (7)	V5—O10^{i}	1.921 (8)
V1—O22^{i}	2.404 (12)	V6—O1	1.598 (7)
V2—O7	1.578 (7)	V6—O3	1.822 (6)
V2—O10	1.744 (8)	V6—O9	1.849 (7)

V2—O13	1.868 (9)	V6—O5	1.867 (7)
V2—O9	1.966 (7)	V6—O4	1.887 (6)
V2—O3	2.036 (7)	V7—O17	1.589 (6)
V2—O21	2.470 (11)	V7—O12	1.806 (7)
V3—O8	1.598 (6)	V7—O18	1.810 (7)
V3—O12	1.821 (7)	V7—O4	1.984 (7)
V3—O13^{i}	1.854 (9)	V7—O5	2.003 (6)
V3—O19^{i}	1.906 (8)	V7—O23^{i}	2.376 (11)
V3—O6	1.933 (7)	P—O22	1.479 (11)
V3—O22^{i}	2.467 (11)	P—O22^{i}	1.479 (11)
V4—O16	1.589 (6)	P—O23	1.552 (11)
V4—O14	1.756 (7)	P—O23^{i}	1.552 (11)
V4—O19	1.797 (9)	P—O20	1.558 (11)
V4—O5	2.007 (7)	P—O20^{i}	1.558 (11)
V4—O3	2.033 (6)	P—O21	1.566 (10)
V4—O21	2.425 (12)	P—O21^{i}	1.566 (10)
V5—O11^{i}	1.922 (8)		

Table S5 Selected bond angles [°] for compound **2**.

Bond angles [°]		Bond angles [°]	
O15—V1—O6	101.3 (4)	O2—V5—O18	100.1 (4)
O15—V1—O11	99.0 (4)	O2—V5—O14	100.8 (4)
O6—V1—O11	96.7 (4)	O18—V5—O14	90.2 (4)
O15—V1—O4	99.9 (3)	O2—V5—O10^{i}	97.0 (4)
O6—V1—O4	92.4 (3)	O18—V5—O10^{i}	90.7 (4)
O11—V1—O4	156.9 (3)	O14—V5—O10^{i}	161.7 (5)
O15—V1—O9	97.3 (3)	O2—V5—O11^{i}	98.0 (4)
O6—V1—O9	159.3 (3)	O18—V5—O11^{i}	161.8 (5)
O11—V1—O9	89.1 (3)	O14—V5—O11^{i}	88.1 (4)
O4—V1—O9	75.5 (2)	O10^{i}—V5—O11^{i}	85.3 (3)
O15—V1—O20	155.1 (4)	O2—V5—O20^{i}	155.4 (4)
O6—V1—O20	99.5 (4)	O18—V5—O20^{i}	98.5 (4)
O11—V1—O20	65.1 (4)	O14—V5—O20^{i}	94.9 (4)
O4—V1—O20	92.5 (3)	O10^{i}—V5—O20^{i}	66.8 (4)

O9—V1—O20	64.9 (4)	O11^{i}—V5—O20^{i}	63.6 (4)
O7—V2—O10	103.1 (5)	O1—V6—O3	110.5 (3)
O7—V2—O13	100.1 (5)	O1—V6—O9	110.4 (4)
O10—V2—O13	94.3 (4)	O3—V6—O9	84.7 (3)
O7—V2—O9	100.5 (4)	O1—V6—O5	108.6 (4)
O10—V2—O9	93.0 (3)	O3—V6—O5	84.9 (3)
O13—V2—O9	156.0 (4)	O9—V6—O5	140.8 (4)
O7—V2—O3	97.9 (4)	O1—V6—O4	107.9 (3)
O10—V2—O3	157.9 (4)	O3—V6—O4	141.6 (3)
O13—V2—O3	88.7 (3)	O9—V6—O4	82.4 (3)
O9—V2—O3	76.3 (3)	O5—V6—O4	82.8 (3)
O7—V2—O20	159.3 (4)	O17—V7—O12	103.0 (4)
O10—V2—O20	66.8 (4)	O17—V7—O18	102.4 (4)
O13—V2—O20	98.7 (5)	O12—V7—O18	94.4 (4)
O9—V2—O20	63.5 (3)	O17—V7—O4	99.5 (3)
O3—V2—O20	91.1 (3)	O12—V7—O4	90.4 (3)
O8—V3—O12	99.7 (4)	O18—V7—O4	155.9 (4)
O8—V3—O13^{i}	99.0 (5)	O17—V7—O5	98.3 (3)
O12—V3—O13^{i}	93.4 (4)	O12—V7—O5	156.8 (4)
O8—V3—O19^{i}	99.3 (5)	O18—V7—O5	89.9 (3)
O12—V3—O19^{i}	160.4 (4)	O4—V7—O5	77.0 (2)
O13^{i}—V3—O19^{i}	88.3 (4)	O17—V7—O23^{i}	157.1 (4)
O8—V3—O6	98.0 (4)	O12—V7—O23^{i}	98.0 (4)
O12—V3—O6	87.1 (3)	O18—V7—O23^{i}	66.6 (4)
O13^{i}—V3—O6	162.6 (5)	O4—V7—O23^{i}	89.3 (3)
O19^{i}—V3—O6	85.6 (3)	O5—V7—O23^{i}	63.0 (4)
O8—V3—O21^{i}	158.7 (4)	O22^{i}—P—O23	113.2 (6)
O12—V3—O21^{i}	97.6 (4)	O22—P—O23^{i}	113.2 (6)
O13^{i}—V3—O21^{i}	67.6 (5)	O22—P—O20	111.5 (6)
O19^{i}—V3—O21^{i}	65.0 (4)	O23^{i}—P—O20	107.5 (6)
O6—V3—O21^{i}	95.2 (4)	O22^{i}—P—O20^{i}	111.5 (6)
O16—V4—O14	102.1 (4)	O23—P—O20^{i}	107.5 (6)
O16—V4—O19	100.2 (4)	O22^{i}—P—O21	111.4 (6)
O14—V4—O19	96.8 (4)	O23—P—O21	106.8 (5)
O16—V4—O5	99.0 (3)	O20^{i}—P—O21	105.9 (6)
O14—V4—O5	90.3 (3)	O22—P—O21^{i}	111.4 (6)
O19—V4—O5	157.6 (4)		
O16—V4—O3	96.9 (3)		
O14—V4—O3	158.2 (3)		
O19—V4—O3	90.2 (3)		
O5—V4—O3	76.1 (3)		

O16—V4—O23^{i}	158.2 (3)		
O14—V4—O23^{i}	68.1 (4)		
O19—V4—O23^{i}	100.2 (4)		
O5—V4—O23^{i}	62.8 (4)		
O3—V4—O23^{i}	90.4 (3)		

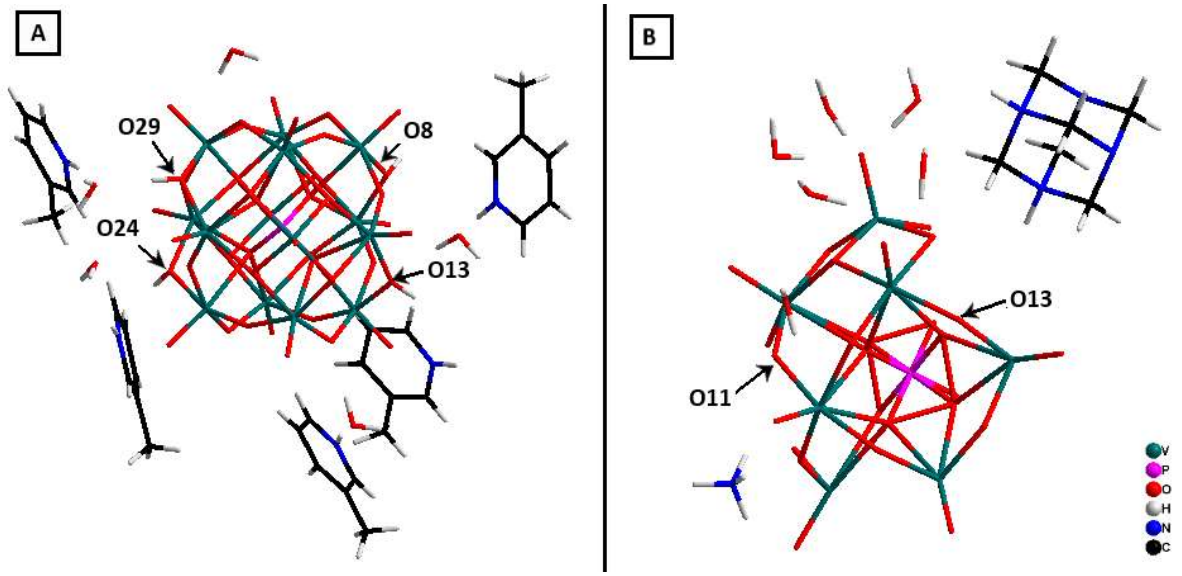

Fig S2 View of the asymmetric unit contents for the crystal structures of compounds **1** and **2**.

Table S6 Hydrogen bonds for compound **1**.

D-H… A	d(D-H)	d(H..A)	<DHA	d(D..A)
N3-HN3…OW2	1.081	1.744	151.92	2.746
O24- HO24…O41[i]	0.690	1.999	165.66	2.673
O13-HO13 ... O21[ii]	0.733	1.975	175.12	2.706
O17-HN2...N2	0.600	2.065	161.57	2.641
OW1-HW2...N1	0.866	2.102	126.75	2.711
N1-HN1 ... OW1	0.895	1.821	172.16	2.711
N5-HN*5... OW3[iii]	1.195	1.499	173.23	2.690
OW5-HWA... OW2	0.868	2.187	116.57	2.690
OW3-HW5... O15	0.911	2.037	157.22	2.899
OW1-HW1... OW3	0.893	1.960	142.62	2.724
OW3-HW6... O19[iv]	1.265	1.507	156.76	2.715
OW3-HW6... O30[v]	1.265	2.479	114.21	3.211
OW2-HW4 ... OW5	0.869	2.014	133.81	2.690
OW2-HW3... O2[vi]	1.047	1.696	153.56	2.674
OW4-HW8... N5[vii]	0.879	2.575	135.74	3.262
OW4-HW7... O12	0.873	2.196	131.98	2.854
OW4-HW7... O32	0.873	2.492	120.89	3.035
N4-HN4... OW4 [viii]	0.869	1.928	160.79	2.764

Symmetry codes : **(i)**: [-x+2, -y+1, -z+1] ;**(ii)**: [x, -y+1/2, z-1/2] ;**(iii)**: [x, -y+1/2, z-1/2] **;(iv)**: [x, -y+1/2, z-1/2] **; (v)**: [x, -y+1/2, z-1/2] ; **(vi)**: [-x+1, -y+1, -z+1] ; **(vii)**: [x, y, z+1]; **(viii)**: [-x+1, -y+1, -z+1].

Table S7 Hydrogen bonds for compound **2**.

D—H···A	D—H	H···A	<DHA	D···A
N3—H4···O16[i]	0.98	2.46	117	3.036 (10)
N3—H4···OW3	0.98	1.95	144	2.805 (13)
N4—H8···O15[ii]	0.98	2.63	118	3.211 (11)
N4—H8···OW5[iii]	0.98	2.12	157	3.047 (13)
N24—H24D···O13	0.98	2.26	127	2.896(16)
N24—H24D···O8 [iv]	0.98	2.34	146	3.135(10)
N24—H24B···O19 [v]	0.98	2.38	126	3.003(13)

Symmetry codes:(i) -*x*+1, -*y*, -*z*+1; **(ii)** *x*+1, *y*, *z*; **(iii)**-*x*+1, -*y*+1,-*z*+1; **(iv)** *x*, *y*-1, *z*; **(v)** 1- *x*,-*y*, -*z*

Powder X-Ray Diffraction data

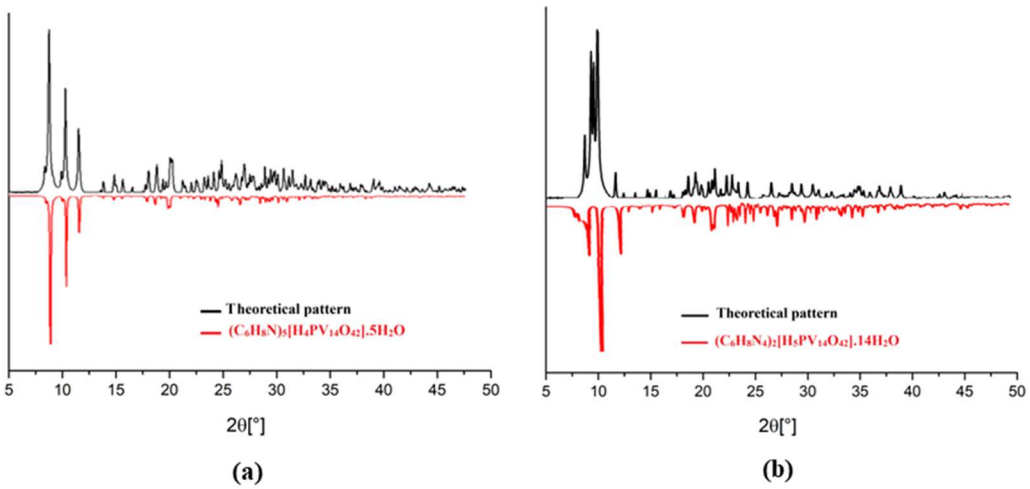

Fig. S3 Powder X-Ray Diffraction pattern of compounds **1** and **2**.

Hirshfeld surfaces Analysis

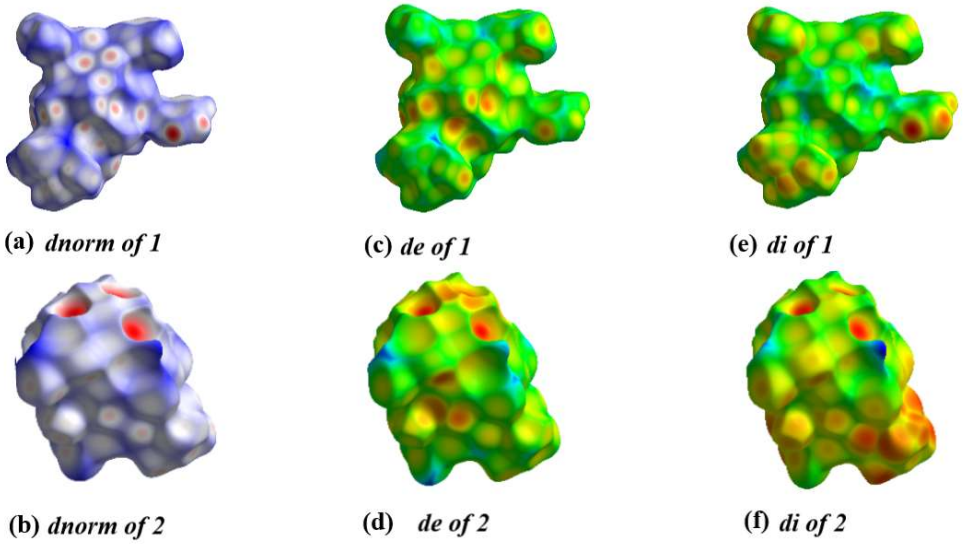

Fig. S4 Hirshfeld surfaces mapped with dnorm, di and de of compounds **1** and **2** mapped over the ranges – 0.717 (red) to 1.467 (blue) for compound **1** and -1.091 (red) to 2.088 (blue) for compound **2**.

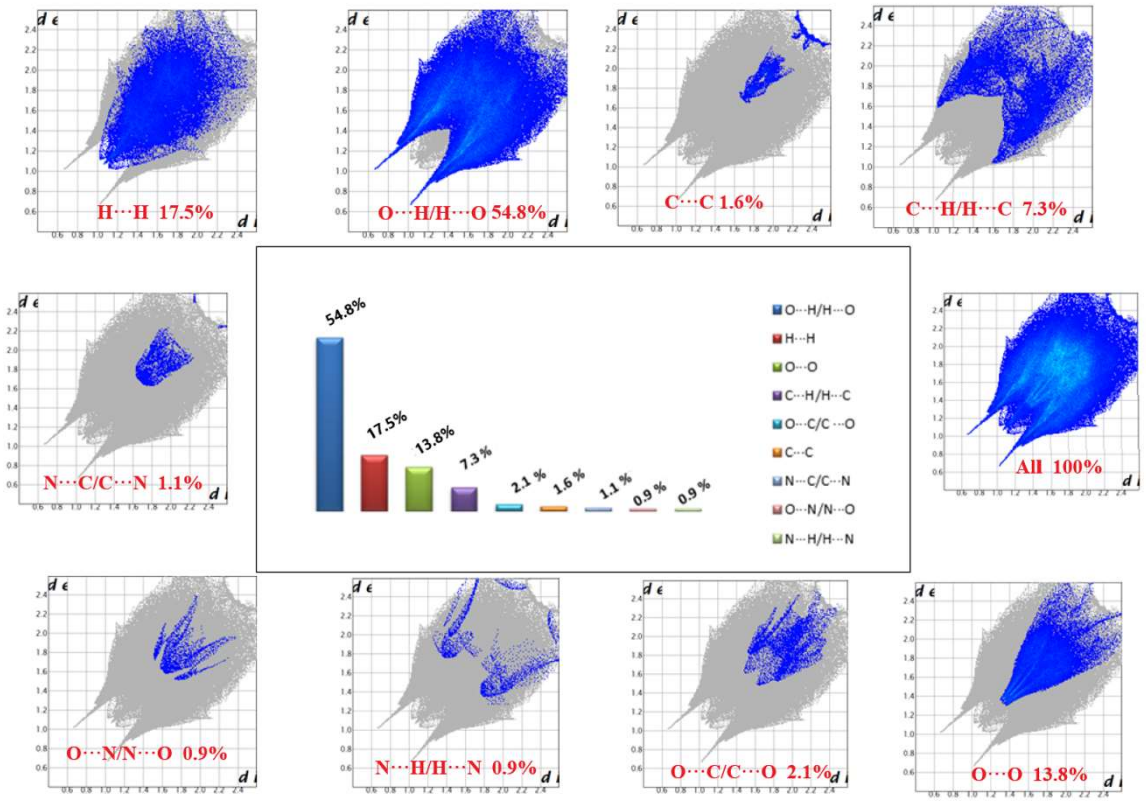

Fig. S5 2D fingerprint plots of **1** where contributions from different contacts may be accessed.

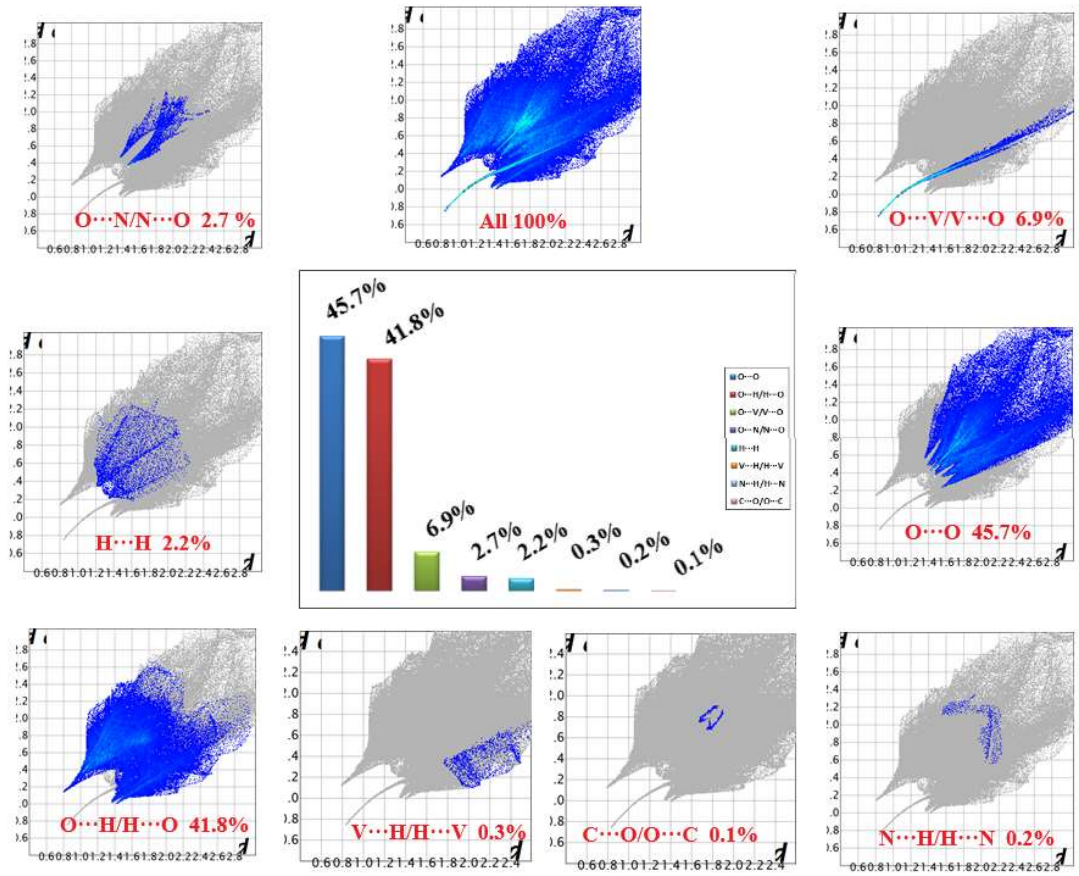

Fig. S6 2D fingerprint plots of **2**.

UV-Vis spectroscopic data

Stability of PV14 compounds at pH = 7 (Hepes buffer) - UV-Vis spectra

Fig. S7 depicts UV-Vis spectra of solutions containing compound **2** in Hepes buffer at several distinct concentrations of PV14.

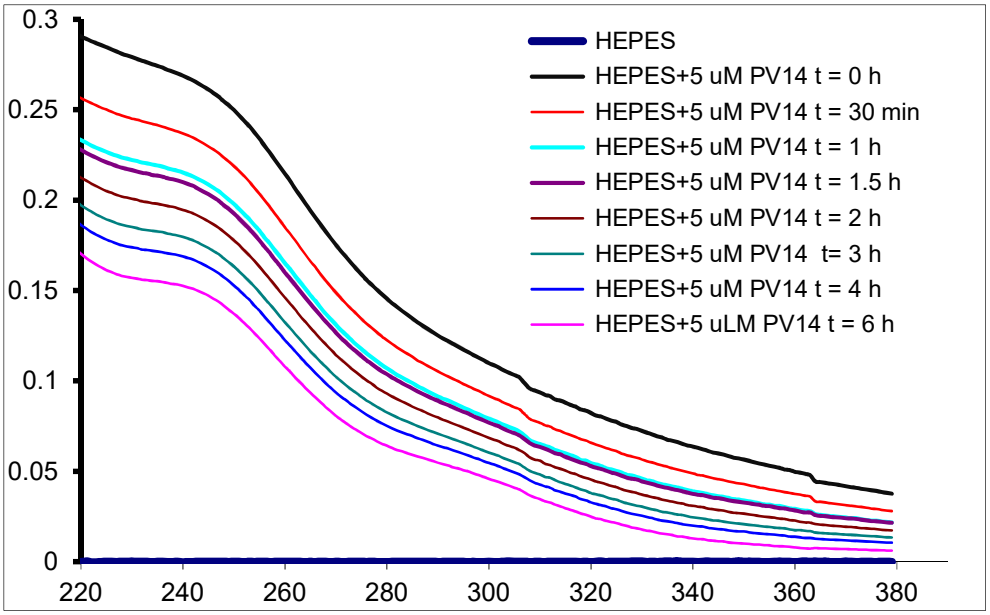

Fig. S7a UV-Vis spectra of compound **2** at a concentration of 5 μM in Hepes buffer at pH = 7.0. Changes of spectra with time at room temperature, path length = 10.0 mm.

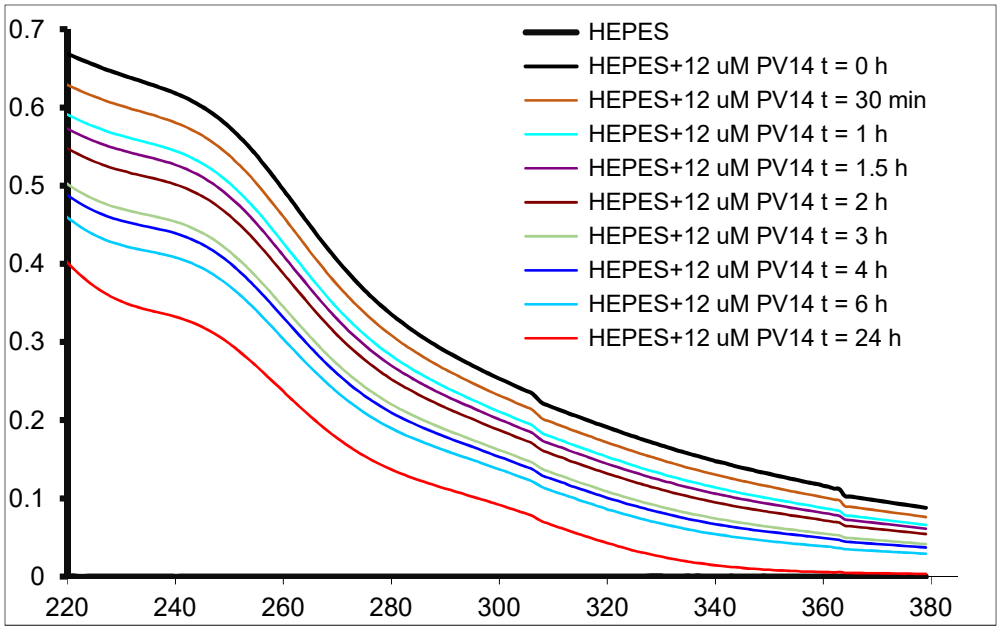

Fig. S7b UV-Vis spectra of compound **2** at a concentration of 12 μM in Hepes buffer at pH = 7.0. Changes of spectra with time at room temperature; path length = 10.0 mm.

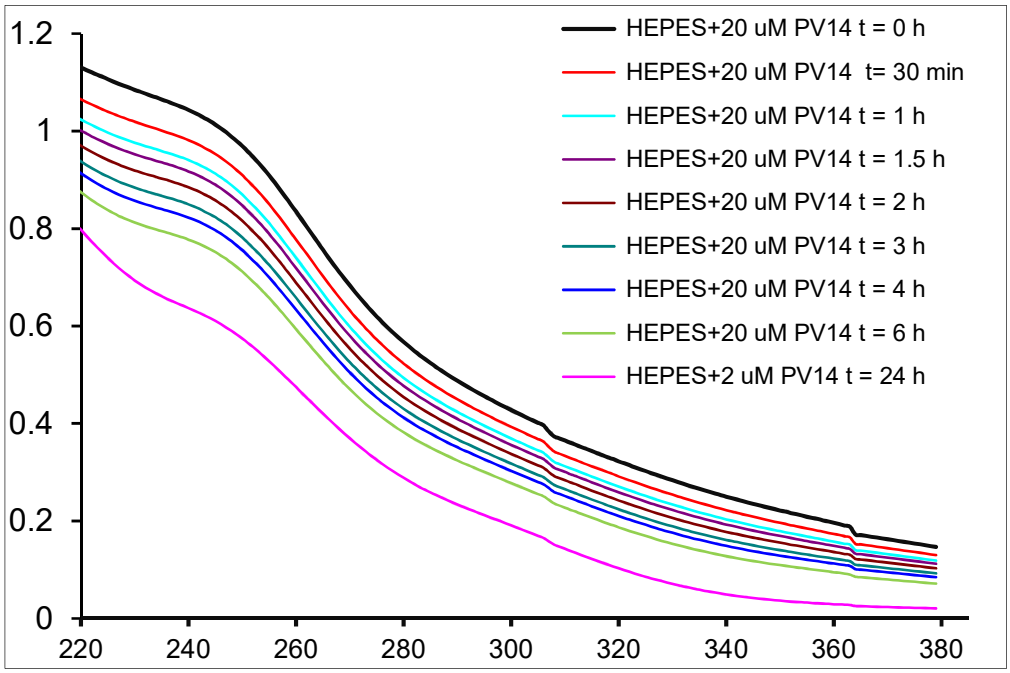

Fig. S7c UV-Vis spectra of compound **2** at a concentration of 20 µM in Hepes buffer at pH = 7.0. Changes of spectra with time at room temperature; path length = 10.0 mm.

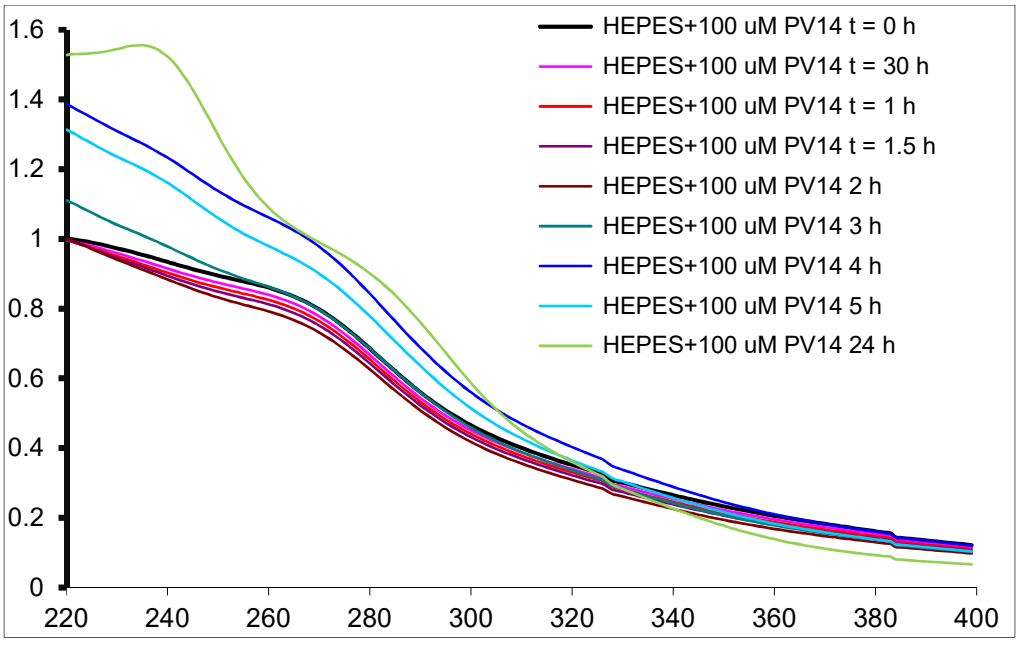

Figure S7d UV-Vis spectra of compound **2** at a concentration of 100 µM in Hepes buffer at pH = 7.0. Changes of spectra with time at room temperature; path length = 2.0 mm. Up to 2 h changes are observed, but for higher periods changes are much more significant, possibly due to precipitation or some other reason.

At pH = 7.0, in Hepes buffer and at low concentration, with time the PV14 polyanion progressively decomposes, yielding mostly V_1, V_2 and V_4, with lower extinction coefficients in the 270-370 nm range. It may be seen that the relative decrease in absorption values with time is higher at lower PV14 concentration, and decreases as the initial PV14 concentrations decrease.

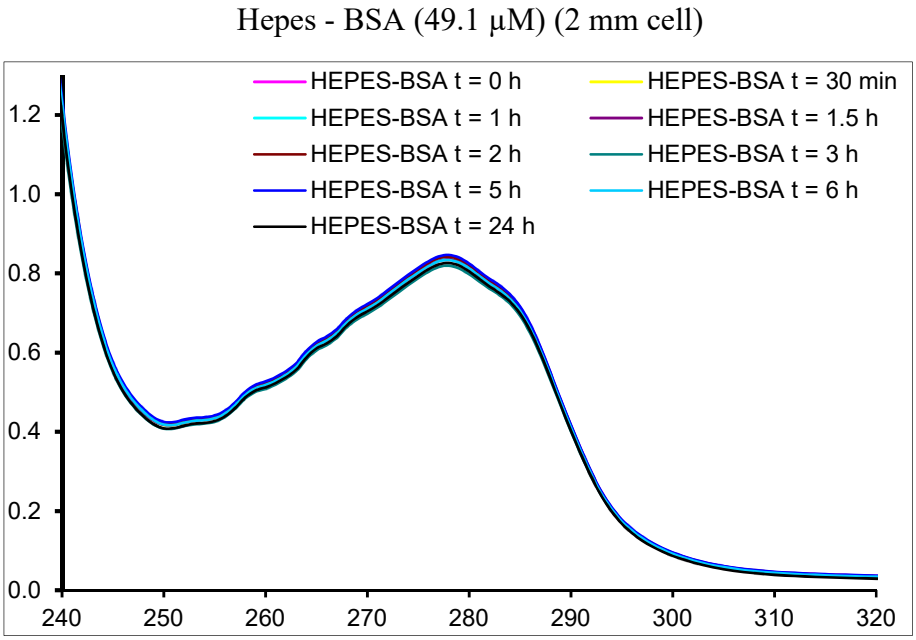

Fig. S8 UV spectra of a solution of BSA at a concentration of 49.1 µM in Hepes buffer at pH = 7.0, recorded with a path length = 2.0 mm. Changes of spectra with time at room temperature.

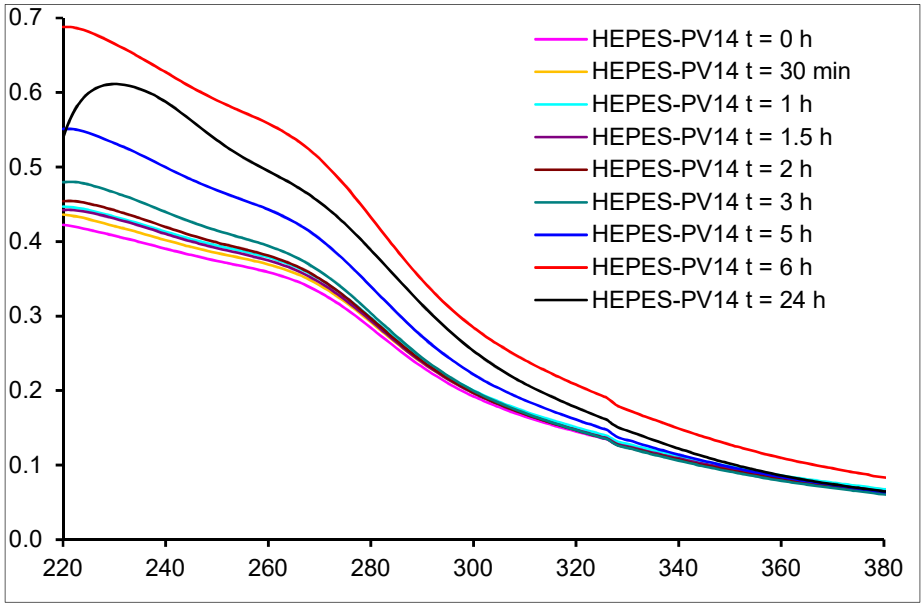

Fig. S9 UV spectra of a solution containing compound **2** (49.1 μM) in Hepes buffer at pH = 7.0, with a path length = 2.0 mm. Changes of spectra with time at room temperature.

HEPES - PV14 (49.1 μM) - BSA (99.8 μM) - (2 mm cell)

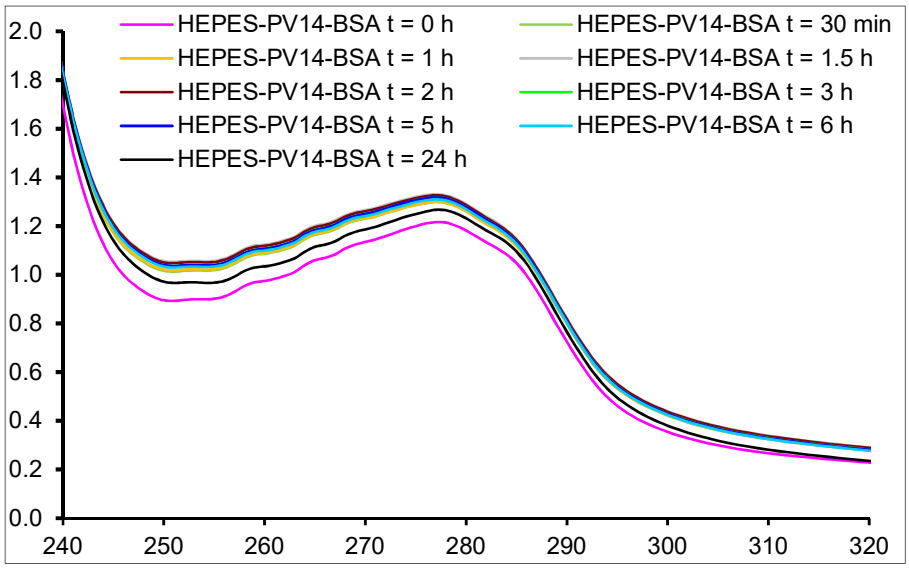

Fig. S10 UV spectra of a solution containing BSA (99.8 μM) and compound **2** (49.1 μM) in Hepes buffer at pH = 7.0, with a path length = 2.0 mm. Changes of spectra with time at room temperature.

From the comparison of the spectra of Figs. S7-S10, it appears that the PV14 anions are somewhat stabilised when BSA is present in solution, but because several species may be present in solution, each contributing differently to the absorption, no definite conclusion can be safely concluded. Notwithstanding, clear changes are observed with time, indicating progressive hydrolysis of the polyanion. At lower concentrations of PV14 hydrolysis probably proceeds faster as the relative amounts of PV14 and other species present in solution markedly decrease with the total V concentration. The species distribution diagrams shown below in Figs. S16a-c demonstrate this.

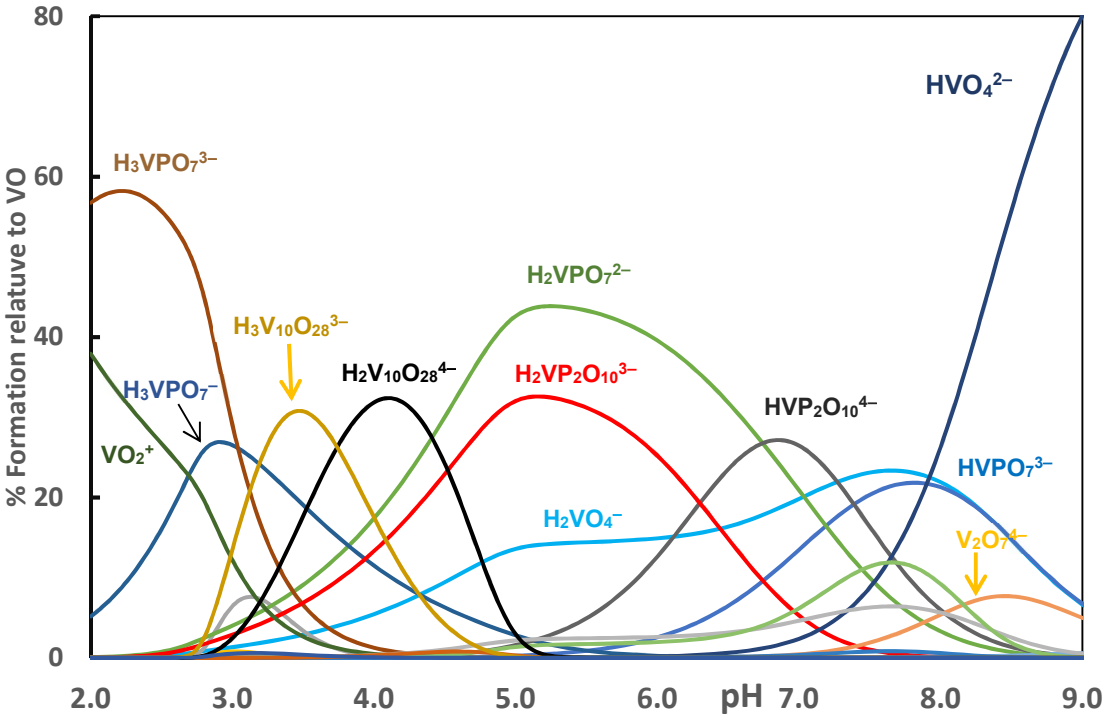

Fig. S11 Species distribution diagrams calculated with the HySS program,[1] with the stability constants from Pettersson and co-workers [2,3] and with [V = $H_2VO_4^-$] = 1×10^{-3} M and [P = $H_2PO_4^-$] at 1×10^{-1} M.

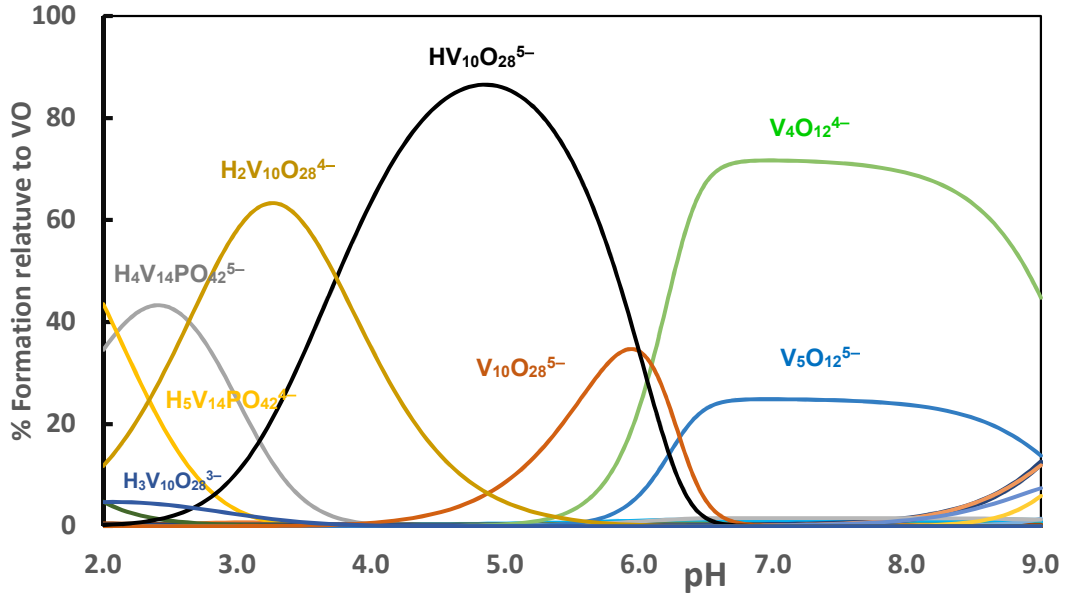

Fig. S12 Species distribution diagrams calculated with the HySS program,[1] with the stability constants from Pettersson and co-workers [2,3] and with [V = $H_2VO_4^-$] = 1×10^{-1} M and [P = $H_2PO_4^-$] at 1×10^{-2} M.

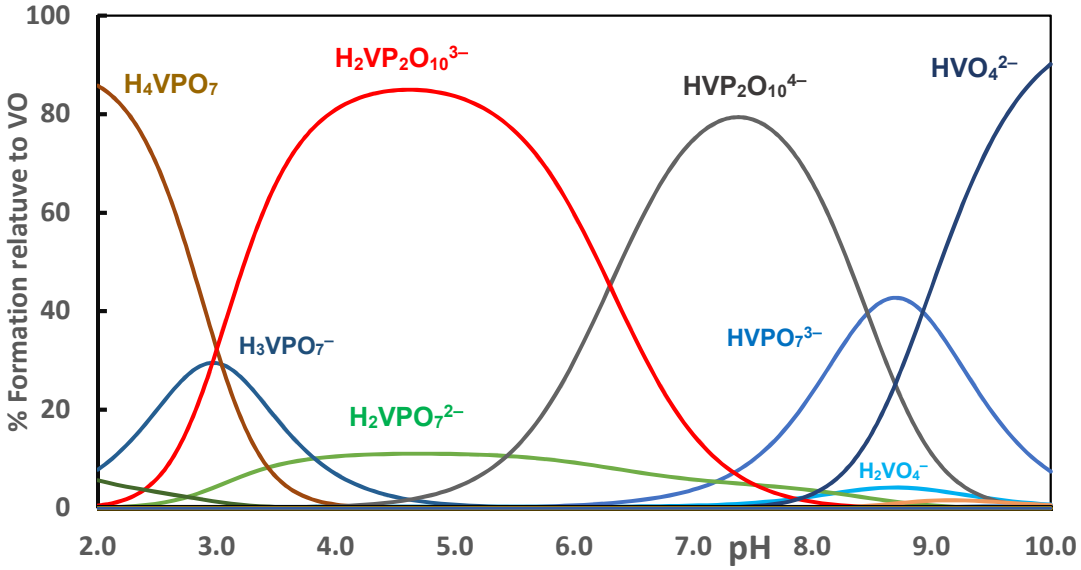

Fig. S13 Species distribution diagrams calculated with the HySS program,[1] with the stability constants from Pettersson and co-workers [2,3] and with [V = $H_2VO_4^-$] = 1×10^{-3} M and [P = $H_2PO_4^-$] at 1 M.

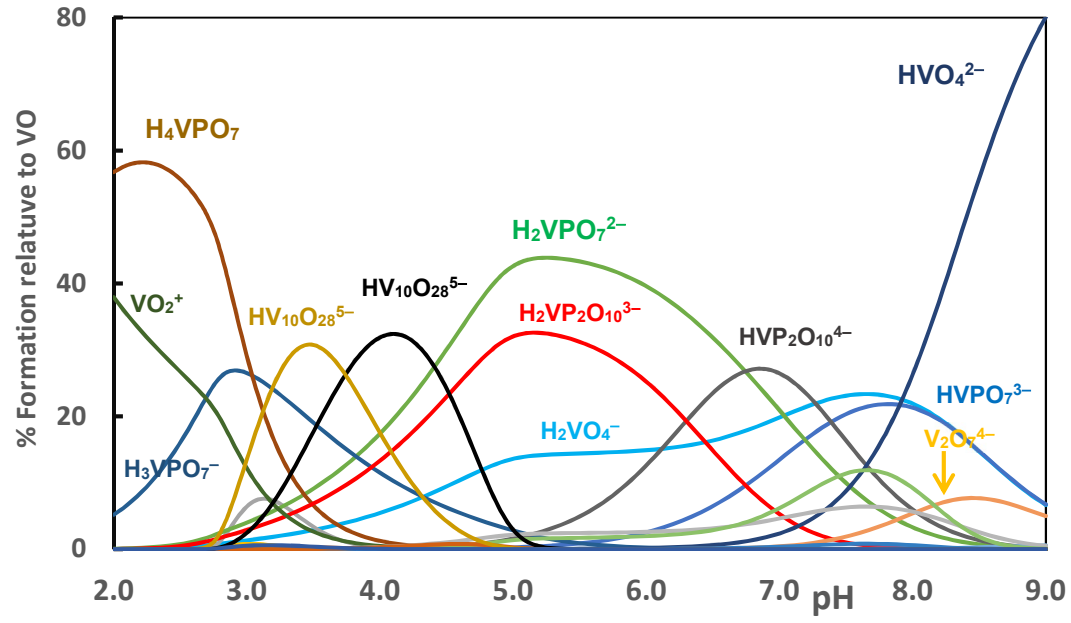

Fig. S14 Species distribution diagrams calculated with the HySS program,[1] with the stability constants from Pettersson and co-workers [2,3] and with [V = $H_2VO_4^-$] = 1×10^{-3} M and [P = $H_2PO_4^-$] at 0.1 M.

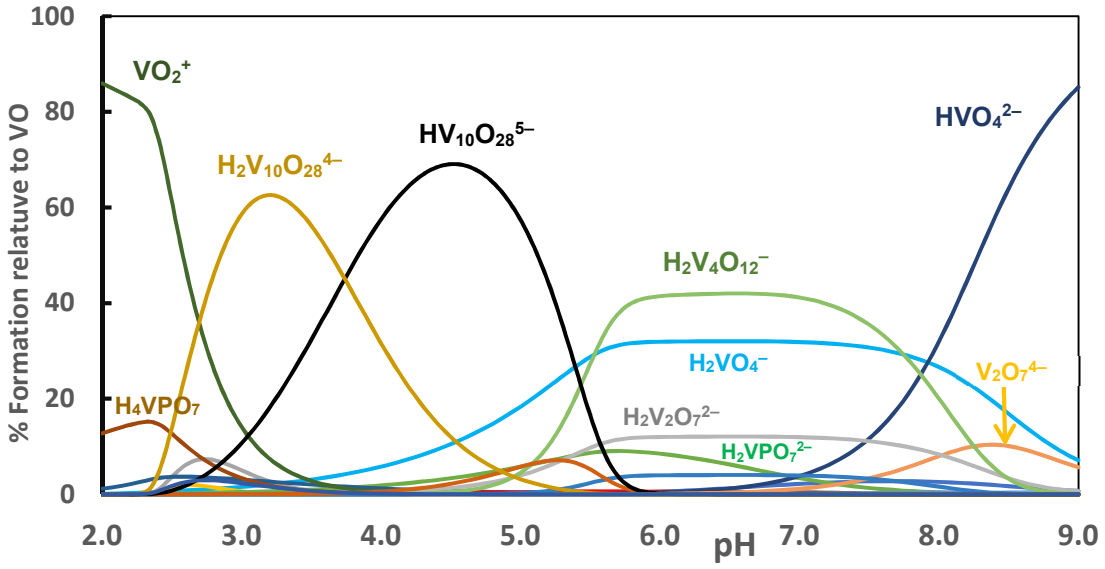

Fig. S15 Species distribution diagrams calculated with the HySS program,[1] with the stability constants from Pettersson and co-workers [2,3] and with [V = $H_2VO_4^-$] = 1×10^{-3} M and [P = $H_2PO_4^-$] at 1×10^{-2} M.

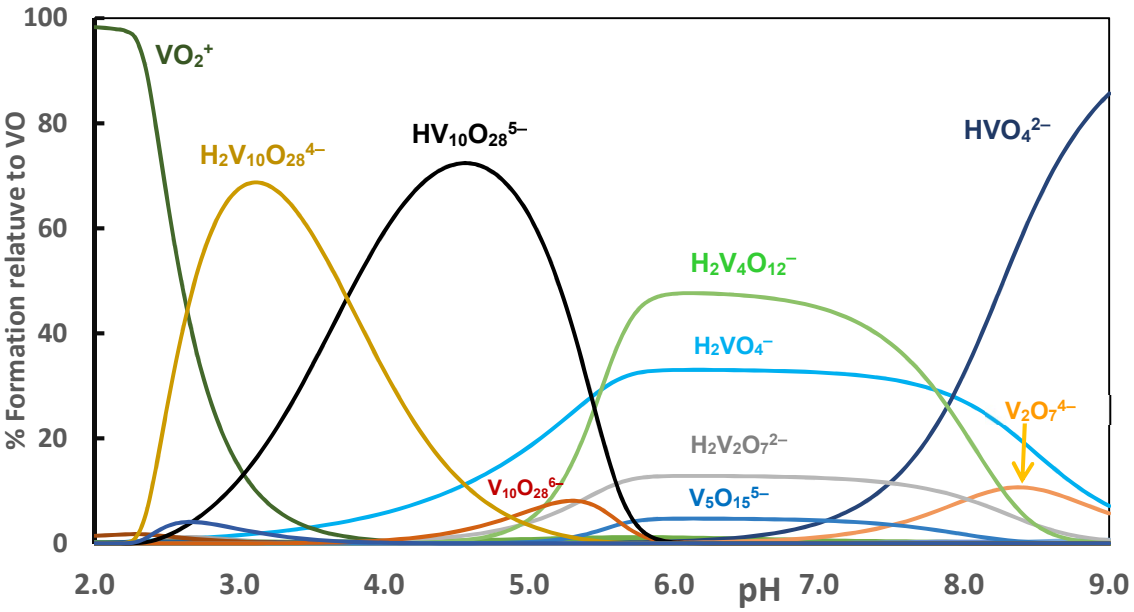

Fig. S16 Species distribution diagrams calculated with the HySS program,[1] with the stability constants from Pettersson and co-workers [2,3] and with [V = $H_2VO_4^-$] = 1×10^{-3} M and [P = $H_2PO_4^-$] at 1×10^{-3} M.

Fluorescence spectroscopy data

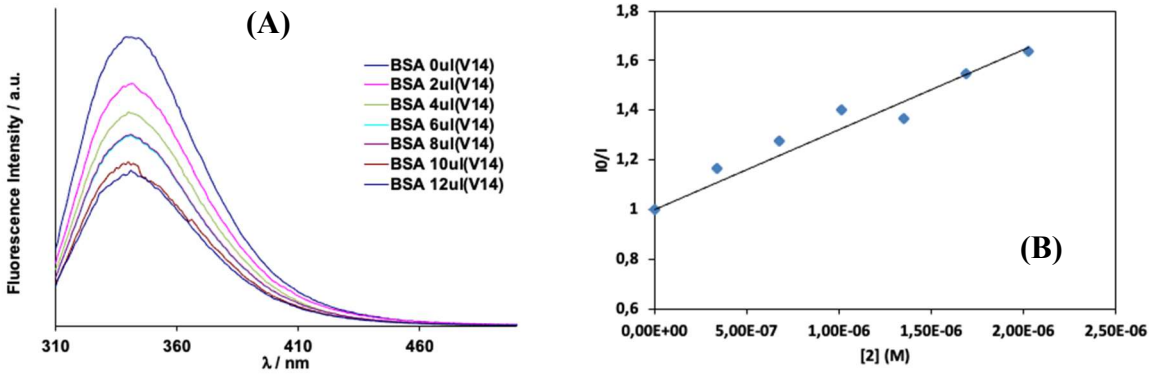

Fig. S17 Fluorescence emission spectra recorded at room temperature for solutions containing BSA (1.5 μM) and increasing amounts of **2** (0.33 – 2.02 μM) with λ_{exc} = 340 nm, in HEPES buffer 10 mM, pH 7.1. The inset shows the variation of % fluorescence intensity at the maximum λ_{em} = 340 nm with the compound concentration. (B) Stern Volmer plot at λ_{em} = 340 nm (R^2 = 0.938). Data from a distinct experiment is depicted in Fig. S18.

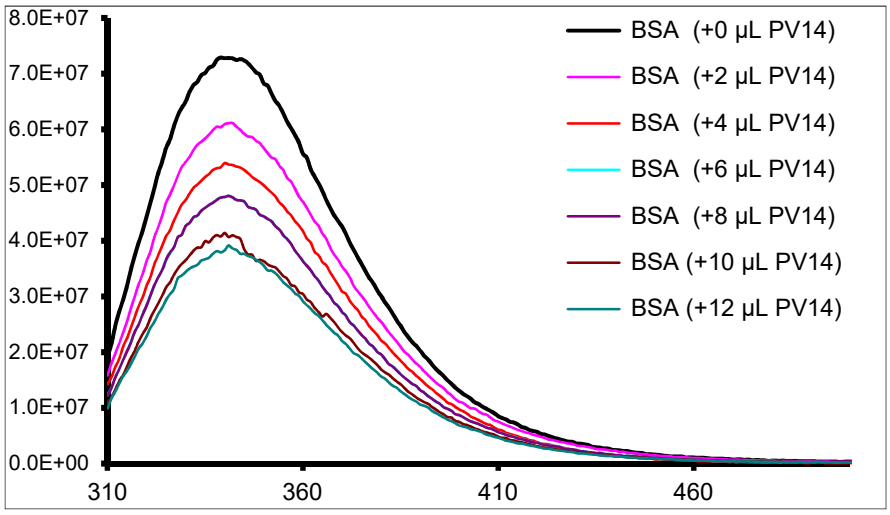

Fig. S18 Fluorescence spectra of solutions containing BSA (1.55 μM) and upon additions of compound **2** (508 μM) in Hepes buffer at pH = 7.0. Each addition of compound **2** corresponds to an increase of the PV14: BSA molar ration of 0.218. Upon addition of 12 μL of **2**, the PV14: BSA molar ratio is 1.31.

The interaction with BSA with 3-picoline and methenamine was also accessed by fluorescence emission spectroscopy. The solution inside the 10×10 mm cell contains *ca.* 1.5 μM of BSA and

additions of small amounts of each amine were done increasing its concentration in small steps up to final ratios amine/BSA of 4.0 and 10.0 for methenamine and 3-picoline, respectively. Blank assays in the absence of BSA were used to subtract the baseline and UV-Vis spectra of each ratio on each titration were also collected to correct the fluorescence emission.

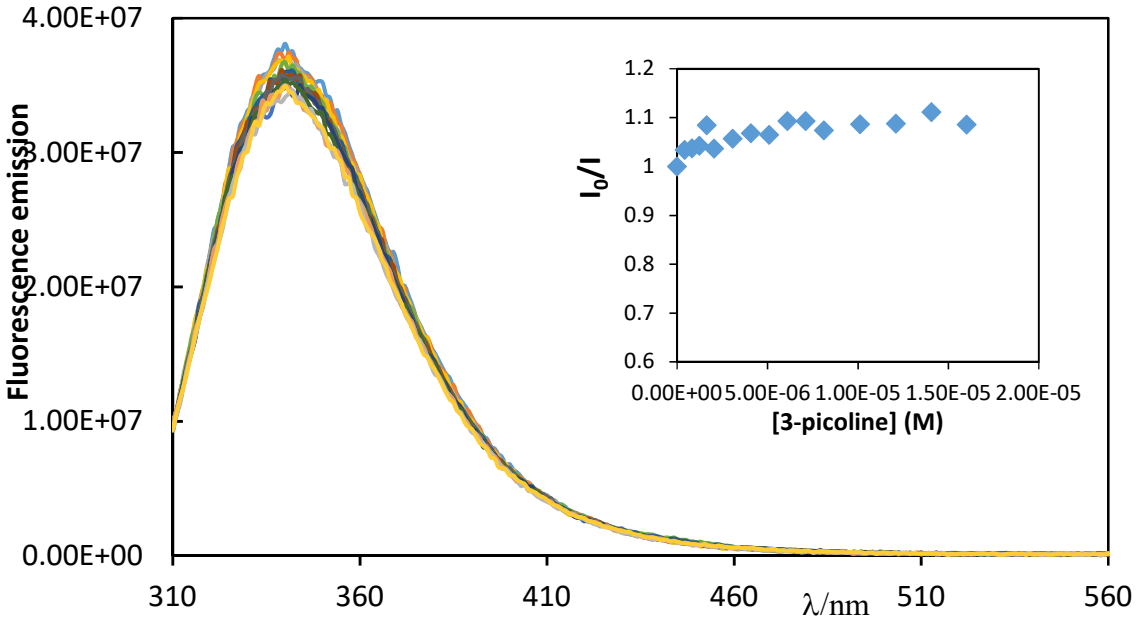

Fig. S19 Fluorescence emission of a 1.6 µM solution of BSA and upon increasing concentrations of 3-picoline (0 – 16.0 µM). The measurements were done in 10 mM Hepes buffer at pH 7.1 and *I*= 150 mM NaCl and using λ_{ex}= 295 nm. The spectra were subtracted of the correspondent blank having the same concentration of the amine in the absence of the protein. The inset depicts the Stern-Volmer plot at 340 nm where it is possible to observe the lack of quenching effect.

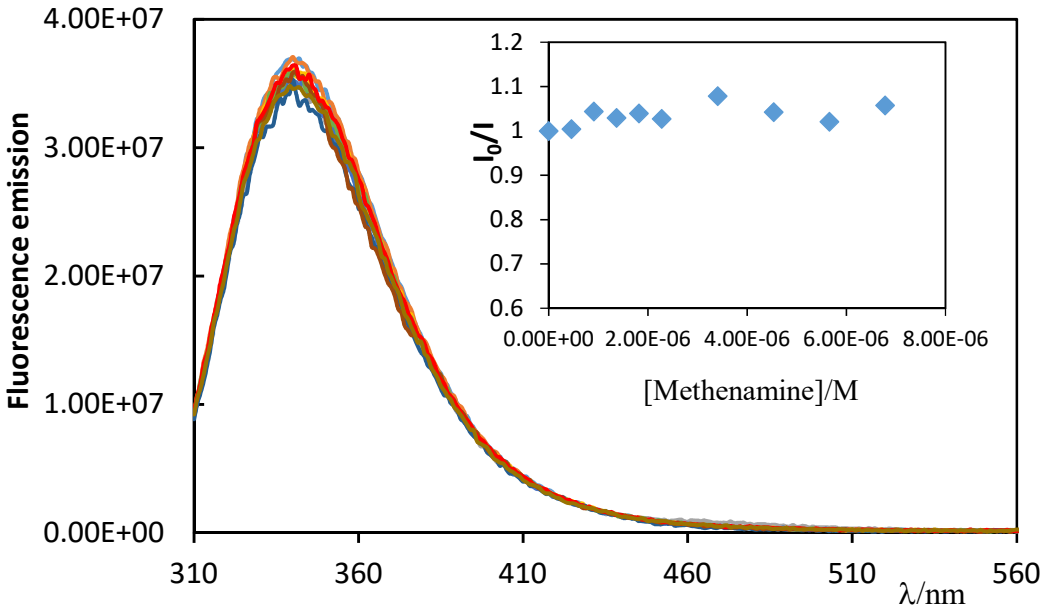

Fig. S20 Fluorescence emission of a 1.6 µM solution of BSA and upon increasing concentrations of methenamine (0 – 6.8 µM). The measurements were done in 10 mM Hepes buffer at pH 7.1 and *I*= 150 mM NaCl and using λ_{ex}= 295 nm. The spectra were subtracted with the correspondent blank having the same concentration of the amine in the absence of the protein. The inset shows the Stern-Volmer plot at 340 nm where it is possible to confirm the lack of quenching effect.

CD spectra with solutions of ctDNA

The CD experiments were done using ctDNA in concentration *ca.* 55 µM· nuc^{-1} in aqueous buffer 10 mM Hepes, 150 mM NaCl and pH 7.1. Stock solutions of methenamine (4 mg/ 5 mL of H_2O) and of 3-picoline (5 µL/ 10 mL H_2O) were added to the 1.0 cm cell in a way that the ratio amine/DNA increases in small steps up to final ratios of 3.0 and 6.0, respectively. Each spectrum is the result of 2 accumulations with a scan speed of 100 nm/min and a resolution of 0.5 nm.

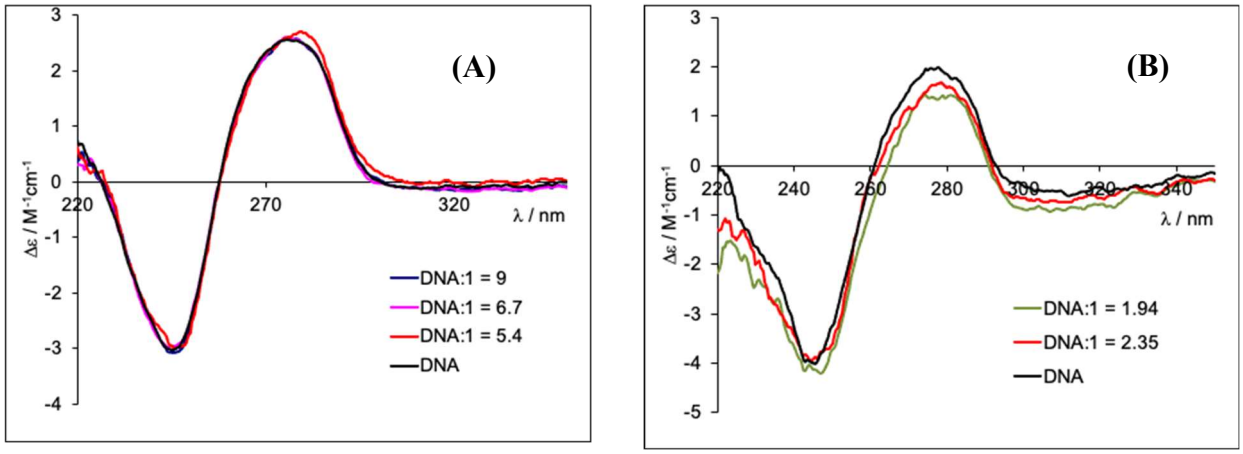

Fig. S21 CD spectra of solutions containing ctDNA in Hepes buffer (10 mM, pH = 7.1) and compound **1** (A) measured with a 10 mm optical path cell, (B) measured with a 5 mm optical path cell. The initial concentration of ctDNA was 54.1 μM nuc^{-1} and a solution of **1** with a concentration of 38.6 μM was progressively added.

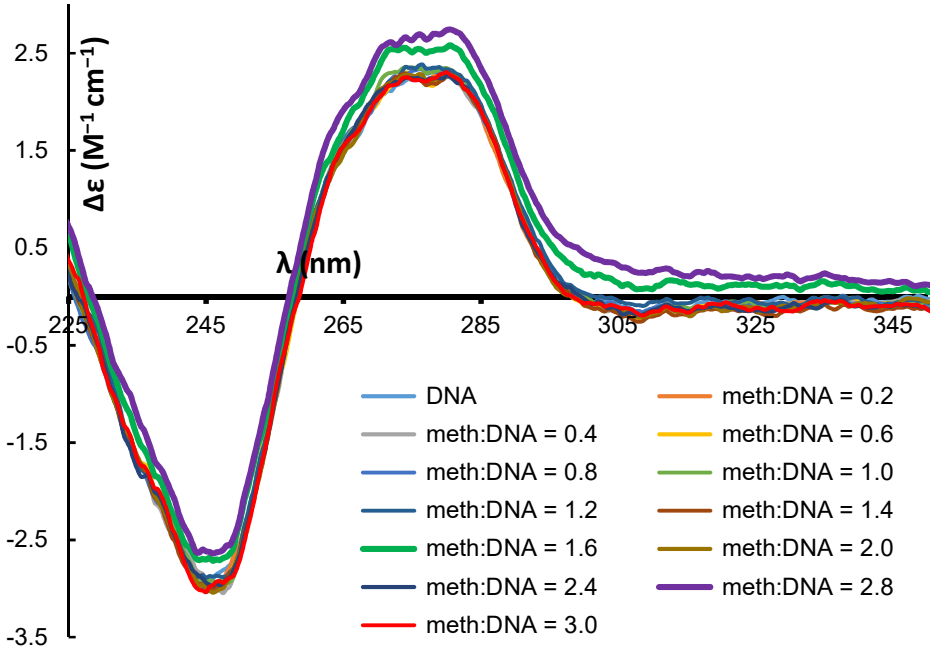

Fig. S22a CD spectra of solutions containing ctDNA in Hepes buffer (10 mM, 150 mM NaCl and pH = 7.1) and methenamine measured with a 10 mm optical path cell. The initial concentration of ctDNA was 59.6 μM nuc^{-1} and a solution of methenamine with a concentration of 5.71 mM was progressively added.

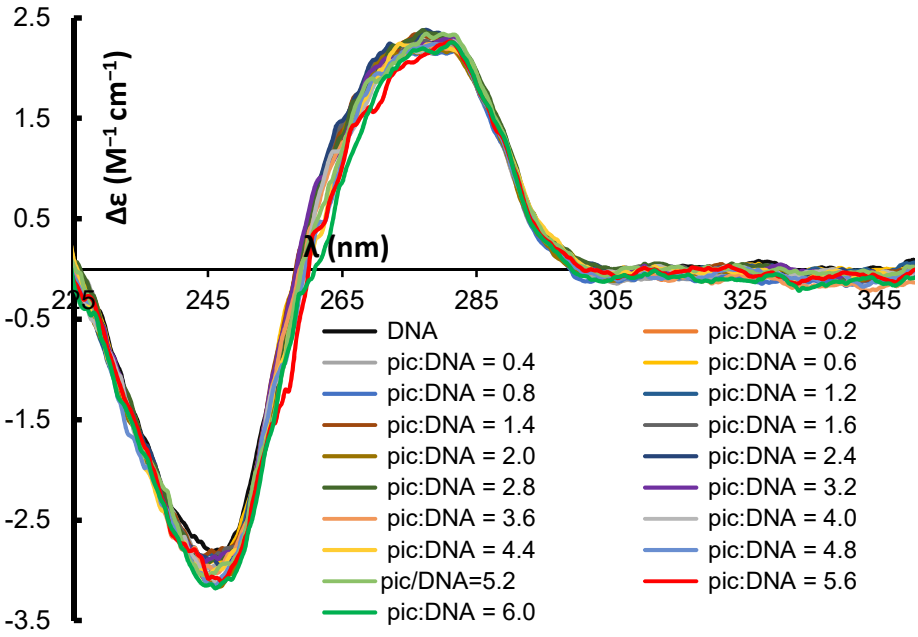

Fig. S22b CD spectra of solutions containing ctDNA in Hepes buffer (10 mM, 150 mM NaCl and pH = 7.1) and 3-picoline measured with a 10 mm optical path cell. The initial concentration of ctDNA was 53.6 μM nuc^{-1} and a solution of 3-picoline with a concentration of 5.14 mM was progressively added.

CD spectra of solutions of CT-DNA with additions of $NaVO_4$

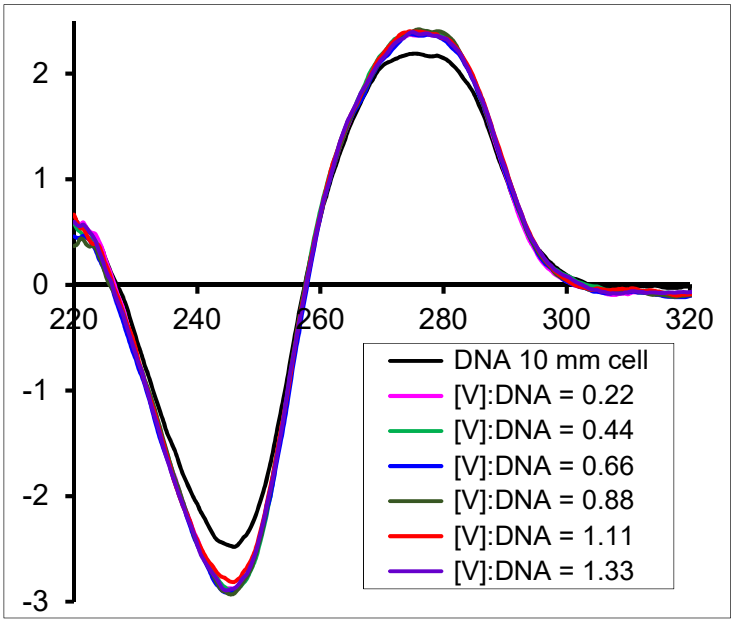

Fig. S23 CD spectra of solutions containing ctDNA in Hepes buffer (10 mM, pH = 7.1) and sodium vanadate measured with a 10 mm optical path cell. The initial concentration of ctDNA was 81.5 μM nuc^{-1} and a solution of sodium vanadate with a concentration of 865 μM was progressively added. No clear trend of changes may be seen in this wavelength range.

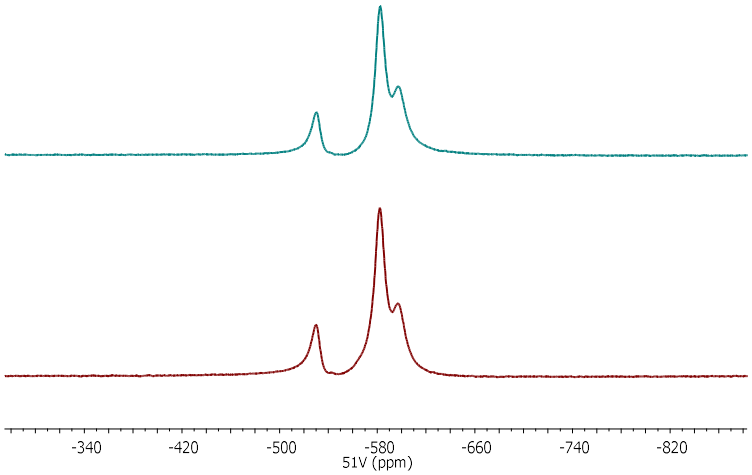

Fig. S24 ^{51}V NMR spectra of compound **1** (*ca*. 6 mM) in D_2O at pH 2.75 at time 0 (top) and after 24 h (bottom).

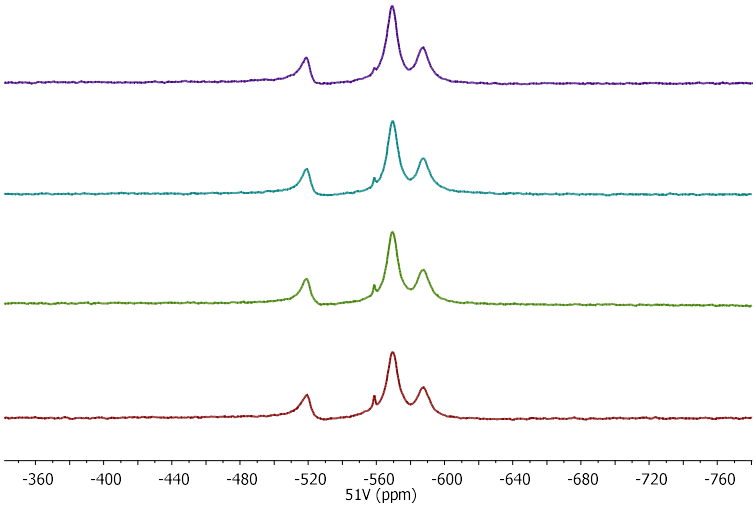

Fig. S25 ^{51}V NMR spectra of compound **1** (0.9 mM) in Hepes buffer (10 mM Hepes, 150 mM NaCl, pH 7.1) at time 0, 3, 6 and 24 h (from top to bottom).

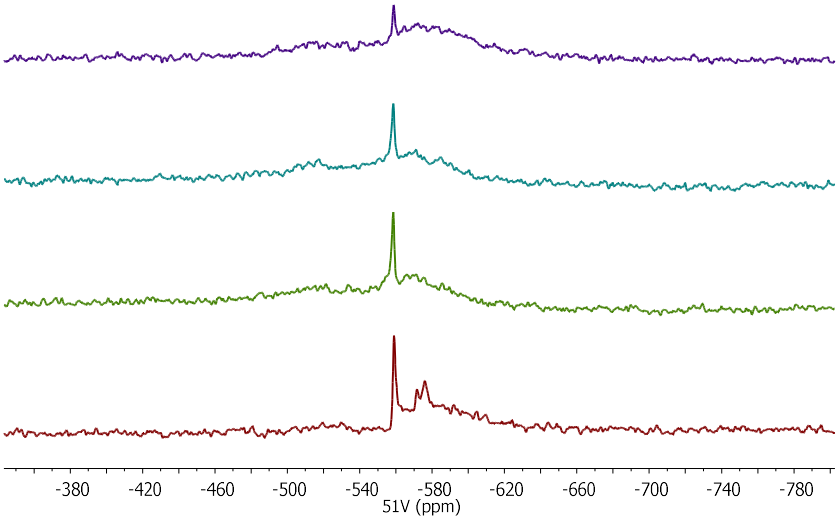

Fig. S26a ^{51}V NMR spectra of compound **1** (0.9 mM) in Hepes buffer (10 mM Hepes, 150 mM NaCl, pH 7.1) at time 0, 3, 6 and 24 h (from top to bottom) in the presence of BSA ([BSA]/[compound]= 0.3).

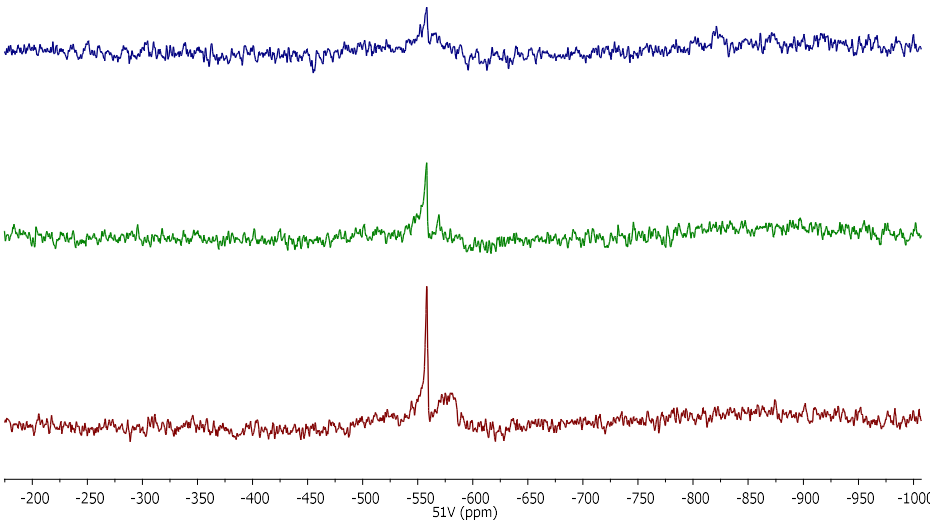

Fig. S26b ^{51}V NMR spectra of compound **1** (0.5 mM) in Hepes buffer (10 mM Hepes, 150 mM KCl, pH 7.1) at time 0 , 3 and 40 h (from top to bottom) in the presence of BSA ([BSA]/[compound] = 1.6).

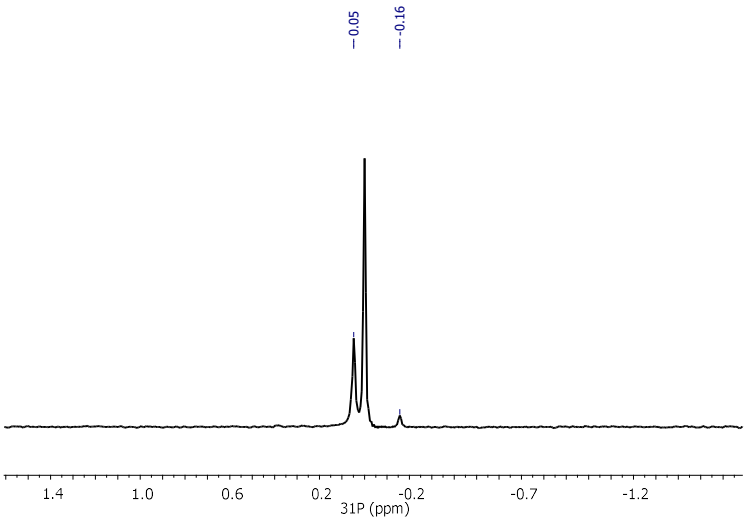

Fig. S27 ^{31}P NMR spectrum of compound **1** (ca. 6 mM) in D_2O at pH 2.75. The signal at 0.0 ppm is 1% H_3PO_4 in D_2O was taken as reference.

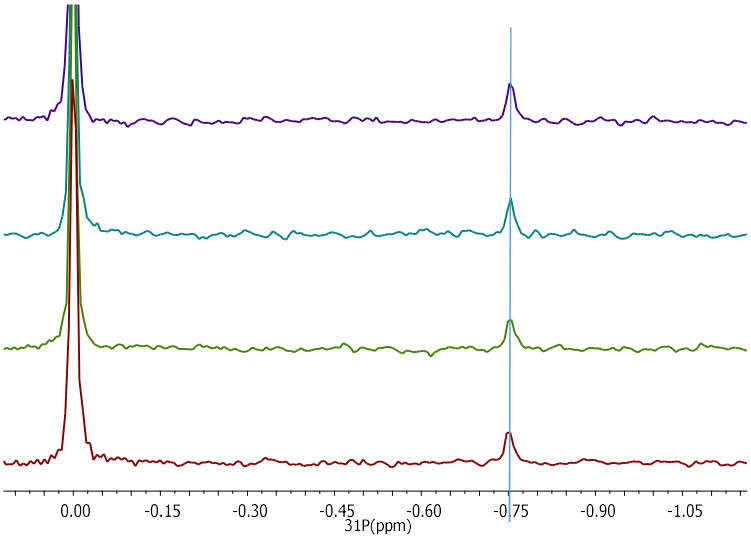

Fig. S28 ^{31}P NMR spectrum of compound **1** (0.9 mM) in Hepes buffer (10 mM Hepes, 150 mM NaCl, pH 7.1) at time 0 , 3 , 6 and 24 h (from top to bottom). The signal at 0.0 ppm is 1% H_3PO_4 in D_2O was taken as reference.

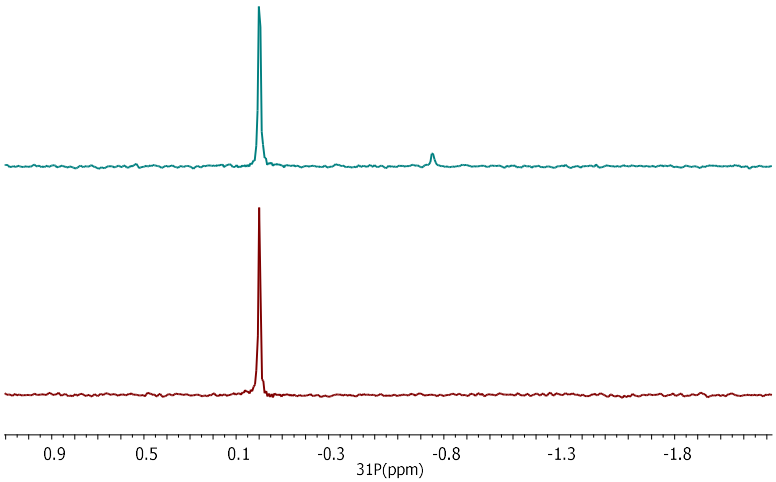

Fig. S29 ^{31}P NMR spectrum of compound **1** (0.9 mM) in Hepes buffer (10 mM Hepes, 150 mM NaCl, pH 7.1) in the absence (top) and in the presence of BSA (bottom, [BSA]/[compound]= 0.3) at time 24 h. The signal at 0.0 ppm is 1% H_3PO_4 in D_2O was taken as reference.

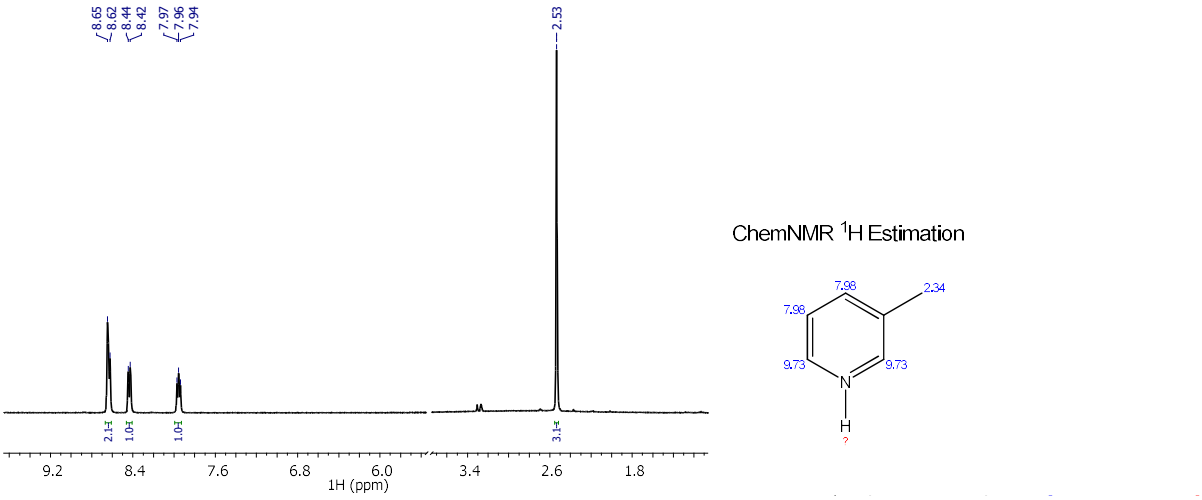

Fig. S30 ^{1}H NMR spectrum of compound **1** (*ca.* 6 mM) in D_2O at pH 2.75 and ^{1}H NMR chemical shifts predicted by ChemBioDraw Ultra (version 11.0.1).

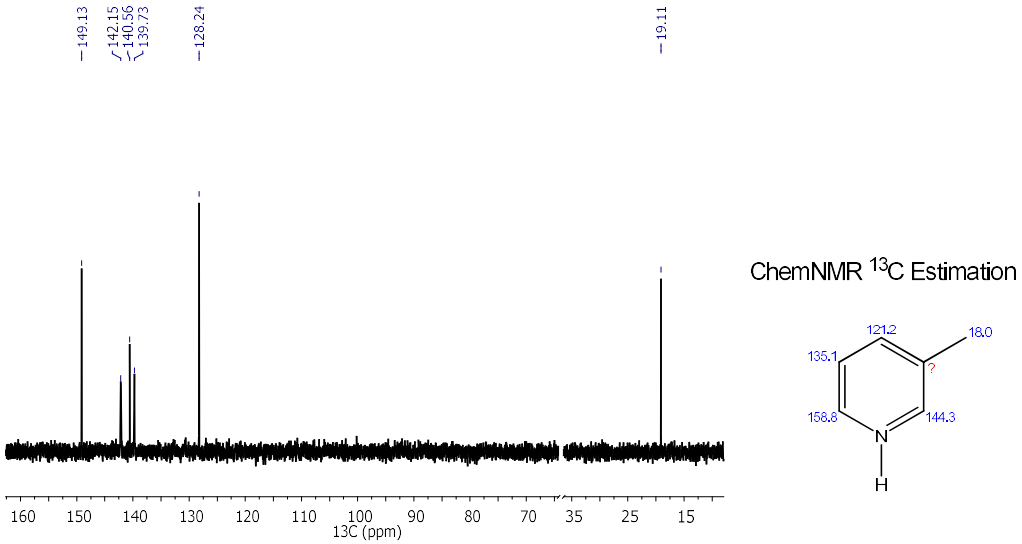

Fig. S31 ^{13}C NMR spectrum of compound **1** (*ca.* 6 mM) in D_2O at pH 2.75 and ^{13}C NMR chemical shifts predicted by ChemBioDraw Ultra (version 11.0.1).

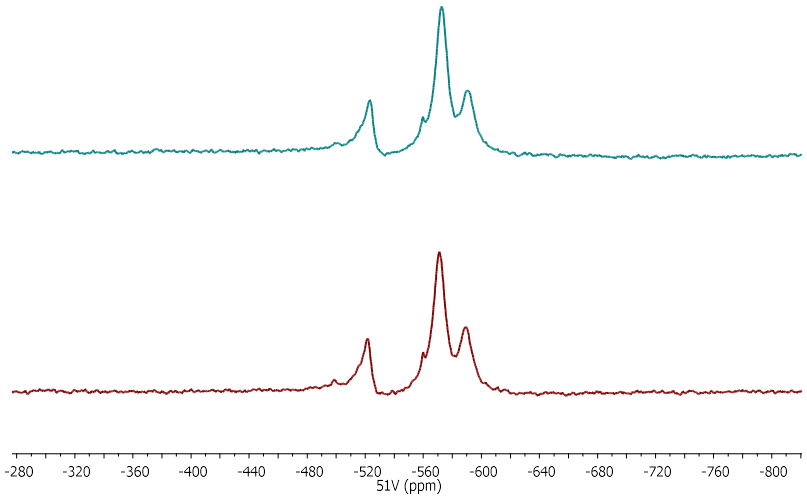

Fig. S32 ^{51}V NMR spectrum of compound **2** (*ca*. 4 mM) in D_2O at pH 2.75 at time 0 (top) and after 24 h (bottom).

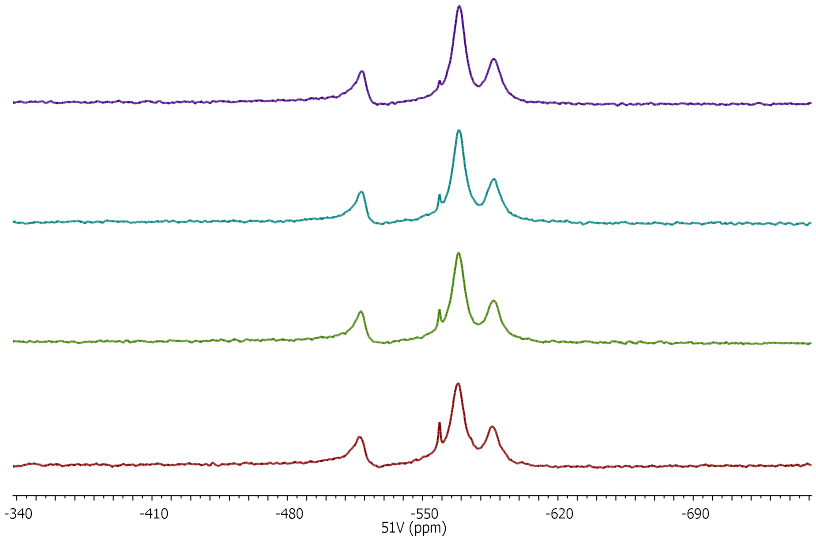

Fig. S33 ^{51}V NMR spectrum of compound **2** (0.9 mM) in Hepes buffer (10 mM Hepes, 150 mM NaCl, pH 7.1) at time 0, 3, 6 and 24 h (from top to bottom).

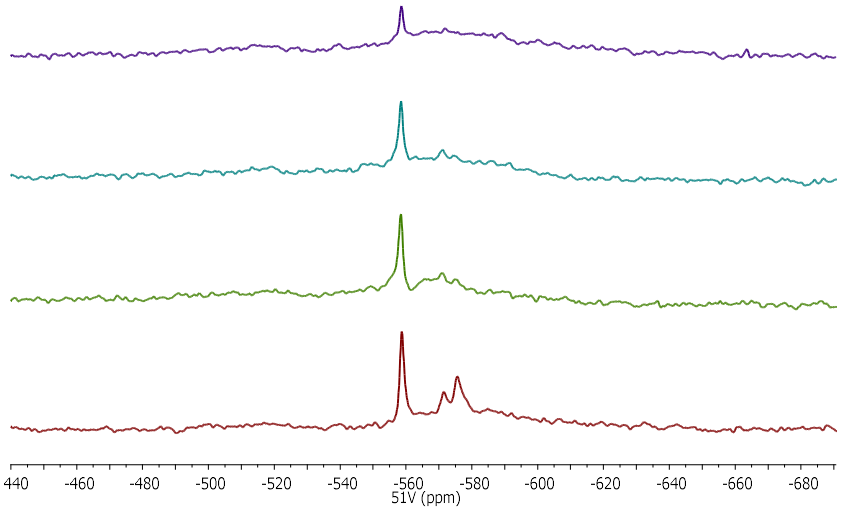

Fig. S34a ^{51}V NMR spectrum of compound **2** (0.9 mM) in Hepes buffer (10 mM Hepes, 150 mM NaCl, pH 7.1) at time 0, 3, 6 and 24 h (from top to bottom) in the presence of BSA ([BSA]/[compound]= 0.3).

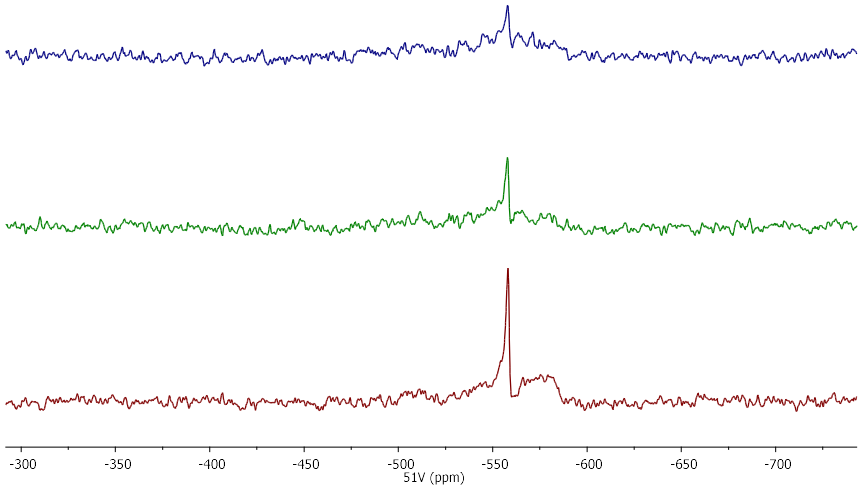

Fig. S34b ^{51}V NMR spectrum of compound **2** (0.5 mM) in Hepes buffer (10 mM Hepes, 150 mM KCl, pH 7,1) at time 0, 3 and 40 h (from top to bottom) in the presence of BSA ([BSA]/[compound]= 1.3).

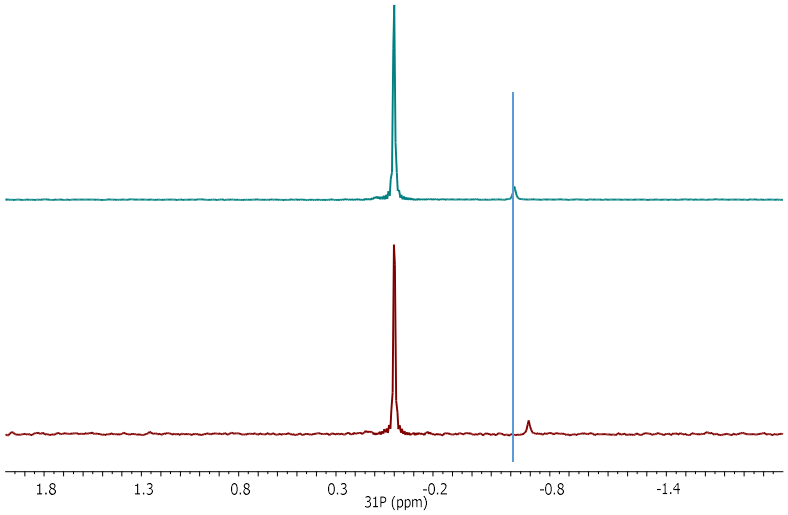

Fig. S35 ^{31}P NMR spectrum of compound **2** (*ca*. 4 mM) in D_2O at pH 2.75 at time 0 h (top) and after 24 h (bottom). The signal at 0.0 ppm is 1% H_3PO_4 in D_2O was taken as reference.

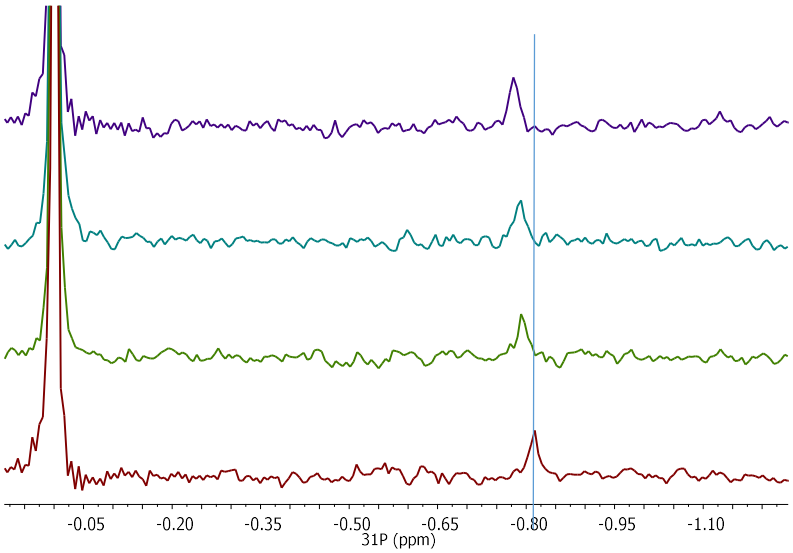

Fig. S36 ^{31}P NMR spectrum of compound **2** (0.9 mM) in Hepes buffer (10 mM Hepes, 150 mM NaCl, pH 7,1) at time 0, 3, 6 and 24 h (from top to bottom). The signal at 0.0 ppm is 1% H_3PO_4 in D_2O was taken as reference.

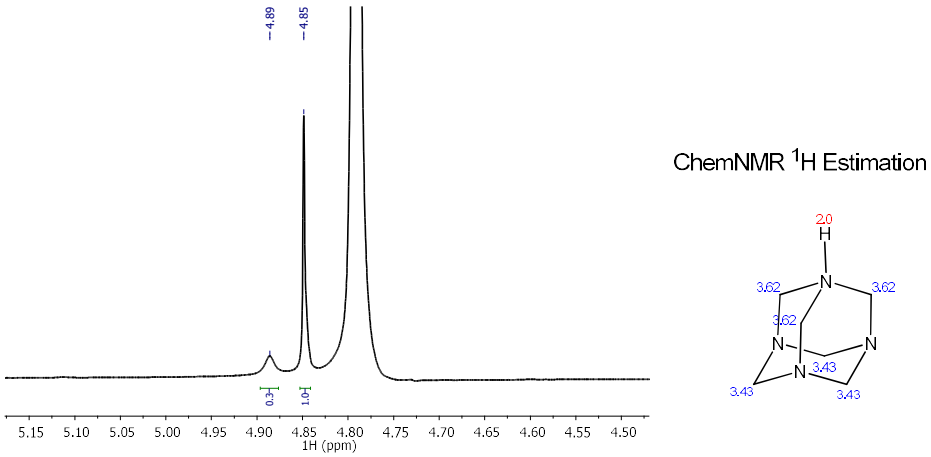

Fig. S37 ^{1}H NMR spectrum of compound **2** (*ca.* 4 mM) in D_2O at pH 2.75 and ^{1}H NMR chemical shifts predicted by ChemBioDraw Ultra (version 11.0.1).

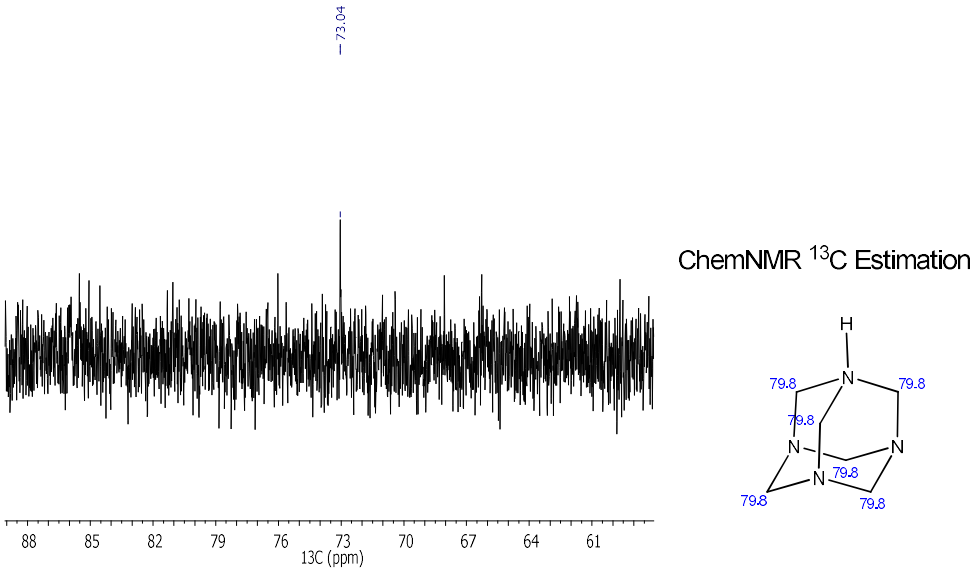

Fig. S38 ^{13}C NMR spectrum of compound **2** (*ca.* 4 mM) in D_2O at pH 2.75 and ^{13}C NMR chemical shifts predicted by ChemBioDraw Ultra (version 11.0.1).

Thermogravimetric analysis of compounds 1 and 2

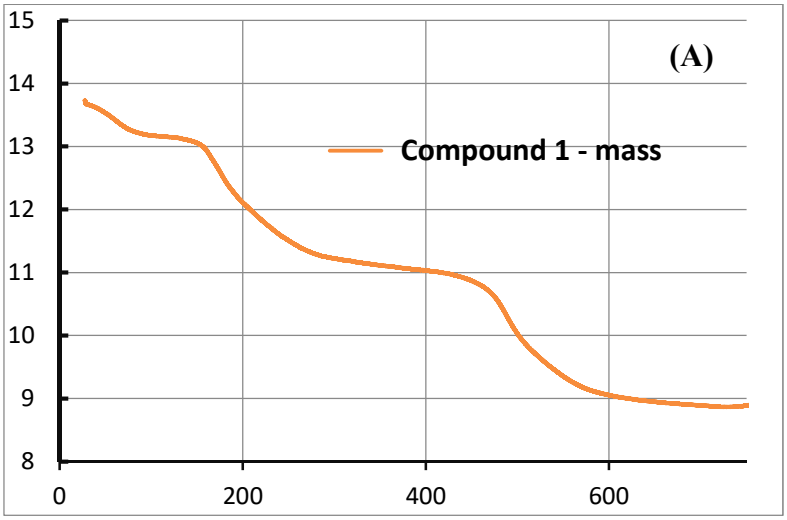

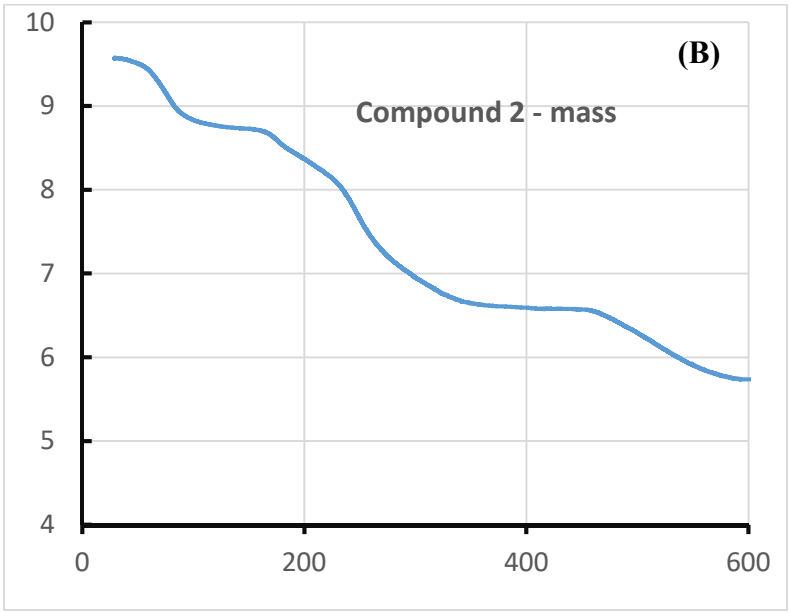

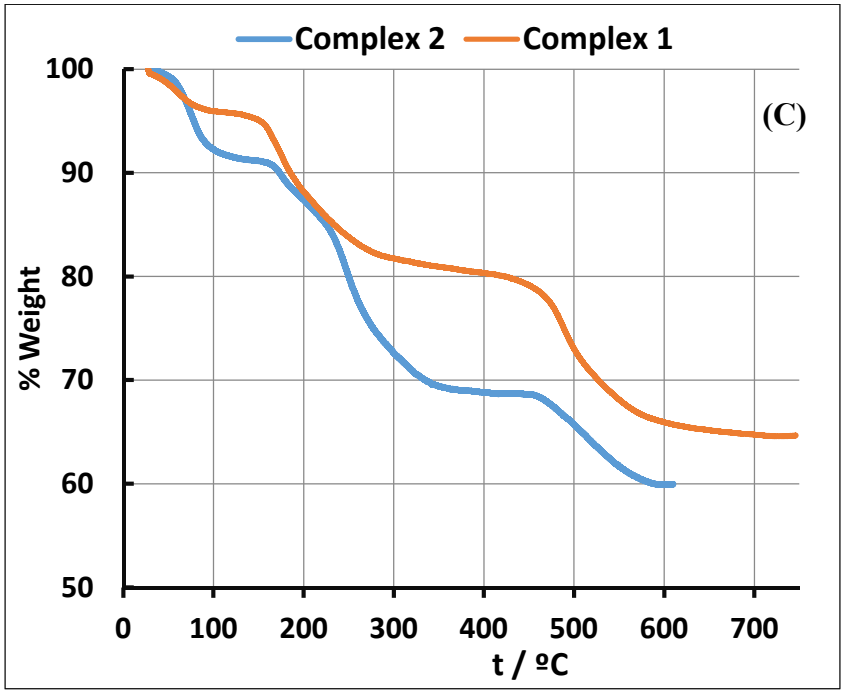

TGA profile for compounds **1**

Fig. S39 Thermograms of compounds **1** (A) and **2** (B) under N_2 atmosphere (see experimental part for details). Fig. (C) corresponds to the thermograms in % of initial masses of compounds **1** and **2**.

The TG of **1** reveals a mass loss of around 5.3% up to 155 ºC. This corresponds to 5 water molecules, which agrees with those determined by SC-XRD. Then, there is a mass loss of ca. 16% up to 400 ºC. The total mass loss of **1** was 35.8 %, the final residue corresponding to 64.2 %. The composition of this residue was not determined. Many phosphorous compounds in TG experiments loose totally their mass up to 600-700 ºC [4-6], others not. The final residue of vanadium compounds at ca. 700 ºC is typically considered as V_2O_5. If this is assumed the final amount of this vanadium oxide may be used to estimate the %V in compound **1**, yielding 36.0%, matching what is expected in its formulation: $\{(C_6H_8N)_5[H_4PV_{14}O_{42}]\cdot 5H_2O\}$. The organic moieties and probably the phosphorous are lost in two steps (1st: 160-300 ºC; 2nd 400-650 ºC), but these cannot be correlated with the composition of compound 1 in a straightforward fashion.

The TG of **2** reveals a mass loss of around 10.3% up to 170 ºC. This corresponds to 10.8 water molecules, which agrees with those determined by SC-XRD. Then, there is a mass loss of ca. 22% up to 450 ºC due to the organic cations and other components of **2**. The final residue at ca. 600 ºC corresponds to ca. 60% of the initial mass. As in the case of **1** the composition of this residue was not determined, but if we assume it corresponds to V_2O_5 If this is assumed the final amount of this

vanadium oxide may be used to estimate the %V in compound **1**, yielding ~31.0%, lower than that expected (37%). The only explanation we may find for this discrepancy is that the sample used for TG analysis was not of the same batch as the crystals used in SC-XRD and in most other experiments.

References

1 L. Alderighi, P. Gans, A. Ienco, D. Peters, A. Sabatini and A. Vacca, *Coord. Chem. Rev.*, 1999, **184**, 311-318.

2 I. Andersson, A. Gorzsas, C. Kerezsi, I. Tóth and L. Pettersson, *Dalton Trans.*, 2005, 3658-3666.

3 A. Selling, I. Andersson, L. Pettersson, C. M. Schramm, S. L. Downey and J. H. Grate, *Inorg. Chem.*, 1994, **33**, 3141–3150.

4 J. C. Markwart, A. Battig, L. Zimmermann, M. Wagner, J. Fischer, B. Schartel and F. R. Wurm, *ACS Appl. Polym. Mater.*, 2019, **1**, 1118-1128.

5 K. A. Salmeia, F. Flaig, D. Rentsch and S. Gaan, *Polymers*, 2018, **10**, 740

6 X. Lai, J. Qiu, H. Li, X. Zeng, S. Tang, Y. Chen and Z. Chen, *Int. J. Pol. Sci.*, 2015, 360274